

Beyond Barren Plateaus: Quantum Variational Algorithms Are Swamped With Traps

Eric R. Anschuetz¹ and Bobak T. Kiani²

¹MIT Center for Theoretical Physics

²Department of Electrical Engineering and Computer Science, MIT

Abstract

One of the most important properties of classical neural networks is how surprisingly trainable they are, though their training algorithms typically rely on optimizing complicated, nonconvex loss functions. Previous results have shown that unlike the case in classical neural networks, variational quantum models are often not trainable. The most studied phenomenon is the onset of barren plateaus in the training landscape of these quantum models, typically when the models are very deep. This focus on barren plateaus has made the phenomenon almost synonymous with the trainability of quantum models. Here, we show that barren plateaus are only a part of the story. We prove that a wide class of variational quantum models—which are shallow, and exhibit no barren plateaus—have only a superpolynomially small fraction of local minima within any constant energy from the global minimum, rendering these models untrainable if no good initial guess of the optimal parameters is known. We also study the trainability of variational quantum algorithms from a statistical query framework, and show that noisy optimization of a wide variety of quantum models is impossible with a sub-exponential number of queries. Finally, we numerically confirm our results on a variety of problem instances. Though we exclude a wide variety of quantum algorithms here, we give reason for optimism for certain classes of variational algorithms and discuss potential ways forward in showing the practical utility of such algorithms.

1 Introduction

1.1 Motivation

The trainability of classical neural networks via simple gradient-based methods is one of the most important factors leading to their general success on a wide variety of problems. This is particularly exciting given the variety of no-go results via statistical learning theory, which demonstrate that in the worst case these models are *not* trainable via stochastic gradient-based methods [13, 75]. There has been recent hope that variational quantum algorithms—the quantum analogue of traditional neural networks—may inherit these nice trainability properties from classical neural networks. Indeed, in certain regimes [34], training algorithms exist such that the resulting quantum model provably outperforms certain classical algorithms. This would potentially enable the use of quantum models to efficiently represent complex distributions which are provably inefficient to express using classical networks [35].

Unfortunately, such good training behavior is not always the case in quantum models. There have been previous untrainability results for deep variational quantum algorithms due to vanishing gradients [60, 19, 59, 63], and for nonlocal models due to poor local minima [5]; however, no such results were known for shallow, local quantum models with local cost functions. Indeed, there have been promising preliminary numerical experiments on the performance of variational quantum algorithms in these regimes, but typically have relied on good initialization [28] or highly symmetric problem settings [79, 50, 51] to show convergence to a good approximation of the global optimum.

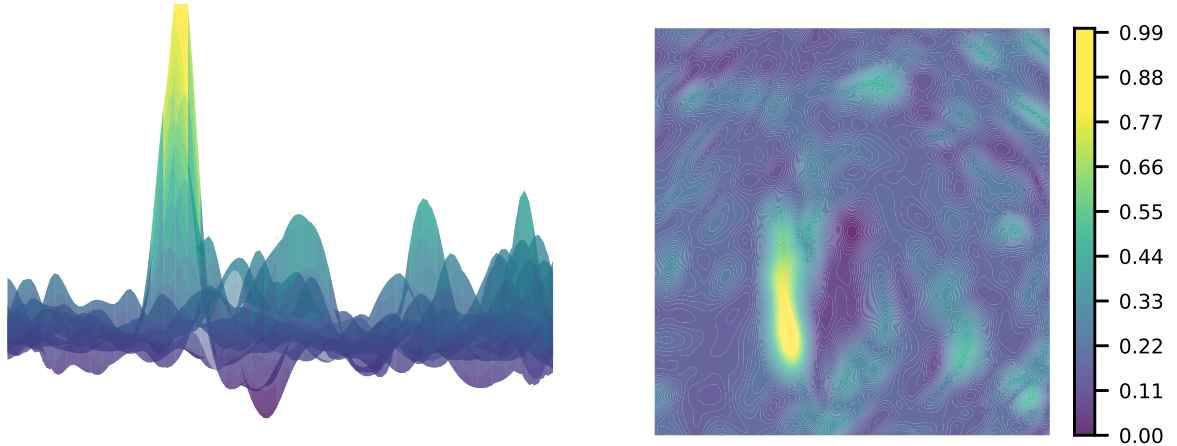


Figure 1: Loss landscapes of underparameterized quantum variational algorithms generally appear “bumpy,” filled with various local minima and traps. Here, we plot the loss landscape as a surface (left) and contour (right) plot along two random normalized directions for the teacher-student learning task of the QCNN for 14 qubits (see Section 5.1). Though a global minimum is located the center of the plot, finding this global minima is generally challenging due to the shape of the loss landscape. Details of this visualization are given in Appendix E.

1.2 Our Contributions

Here, we show that generally such models are *not* trainable, particularly when a good choice of initial point is not known and when the model does not exhibit a high amount of symmetry. Specifically, we generalize results from classical statistical query learning to show that, under worst case noise, such quantum models are not efficiently trainable. We then extend the techniques used in [5] to show that additionally, for typical instances, local minima concentrate far from the global optimum even for certain local shallow circuits that do not suffer from barren plateaus. This phenomenon can be visualized in Figure 1, where the training landscape for a shallow QCNN learning a random instance of itself is shown to concentrate far from the global optimum. As in [5], this phenomenon is the result of a trainability phase transition in the loss landscape of the quantum model. In [5], this transition was governed by the ratio of the number of parameters to the Hilbert space dimension; we show in the shallow case that instead, this transition is governed by the ratio of the *local* number of parameters to the *local* Hilbert space dimension, in the reverse light cone of a given measured observable. As this is typically much less than one for local variational ansatzes, these models are typically untrainable. We then give numerical evidence of this fact, and conclude by studying where there may be reason for optimism in the training of certain variational quantum models.

Our work proceeds as follows. In Section 2, we give background on the techniques we use to study the trainability of variational quantum algorithms. In Section 3, we discuss a quantum statistical query learning framework, and summarize our results proven in the associated Appendix C. Similarly, in Section 4, we informally discuss our results on the training landscapes of shallow variational quantum algorithms, with the detailed statements and proofs in the associated Appendix D. We give numerical evidence of the proven phenomena in Section 5, and finally conclude in Section 6.

2 Preliminaries

2.1 Quantum Machine Learning

Quantum machine learning algorithms have been a focus of intense research effort as potential use-cases for noisy, intermediate-scale quantum (NISQ) [68] devices. Here, we show via simple arguments that access to a more expressive “quantum” space of functions or data is only advantageous when one can efficiently optimize or search over that space. Indeed, there are known results on expressivity advantages of quantum models over classical models [35], and certain learning settings where there is known to exist a quantum advantage in the data needed to learn [43, 1]. Just as in classical machine learning, algorithms are tasked with minimizing some risk:

$$\mathcal{R}(f) = \mathbb{E}_{\mathbf{x}} [\ell(f(\mathbf{x}))], \quad (1)$$

given a model f , a distribution of inputs \mathbf{x} , and a loss function ℓ . To perform learning, one searches for a model $\hat{f} \in \mathcal{F}$ in the function class \mathcal{F} (e.g. the set of functions expressed by quantum neural networks). The expected risk $\mathcal{R}(f)$ is typically not something one can calculate, as it requires access to the full probability distribution of the data. Instead, one often minimizes the empirical risk $\hat{\mathcal{R}}(f)$ (often named the *training error*) over a given training data set \mathcal{D} of size N :

$$\hat{\mathcal{R}}(f) = \sum_{\mathbf{x}_i \in \mathcal{D}} \ell(f(\mathbf{x}_i)). \quad (2)$$

Note that we use the hat in $\hat{\mathcal{R}}$ and \hat{f} to denote the expected risk measure and model that one actually has access to during training or optimization. As we show in Appendix A, one can bound the expected risk of any function \hat{f} as a decomposition into the *approximation*, *generalization*, and *optimization* errors [14]:

$$\mathbb{E} [\mathcal{R}(\hat{f}) - \mathcal{R}(f^*)] \leq \underbrace{\min_{f \in \mathcal{F}} \mathcal{R}(f) - \mathcal{R}(f^*)}_{\text{approximation error}} + \underbrace{2\mathbb{E} \left[\sup_{f \in \mathcal{F}} |\mathcal{R}(f) - \hat{\mathcal{R}}(f)| \right]}_{\text{generalization error}} + \underbrace{\mathbb{E} \left[\hat{\mathcal{R}}(\hat{f}) - \min_{f \in \mathcal{F}} \hat{\mathcal{R}}(f) \right]}_{\text{optimization error}}, \quad (3)$$

where the expectation above is taken with respect to the distribution over training data.

As detailed in Appendix A, the approximation error and generalization error are typically bounded in quantum machine learning since variational models are usually shallow but expressible enough to approximate the target [18, 32]. In fact, previous results on quantum advantage show that the generalization error is bounded with sufficiently more data points than trainable parameters [18, 42, 11]. However, these sample complexity results are only part of the story for quantum machine learning, since the runtime complexity of reducing the optimization error can be unmanageable. This is in contrast with classical deep learning where obtaining tight generalization bounds is highly nontrivial but reducing the optimization error is typically efficient [83]. Thus, here, we focus on the *optimization error*. In fact, in the context of *variational quantum algorithms*, feasibility of optimization has been a major topic of research in recent years, as we summarize in Section 2.2.

2.2 Variational Quantum Algorithms

Variational quantum algorithms (VQAs) [66] are a class of quantum generative models where one expresses the solution of some problem as the smallest eigenvalue and corresponding eigenvector (typically called the *ground state*) of an objective Hermitian matrix \mathbf{H} —called the *Hamiltonian*—on n qubits. Given a choice of generative model—often called an *ansatz* in the quantum algorithms literature:

$$|\boldsymbol{\theta}\rangle = \prod_{i=1}^q \mathbf{U}_i(\theta_i) |\psi_0\rangle \quad (4)$$

Result	Dimension	Locality	Depth	Average case?	Barren plateaus?	Poor minima?
[60]	d	2	$\Omega(n^{\frac{1}{d}})$	✓	✓	?
[19]	1	2	$\omega(\log(n))$	✓	✓	?
[63]	d	2	$\omega(\log(n)^{\frac{1}{d}})$	✓	✓	?
[5]	N/A	n	$\Omega(1)$	✓	✓/✗	✓/✗
[81]	d	2	$\Omega(1)$	✗	?	✓
Our results	d	2	$\Omega(1)$	✓	✗	✓

Table 1: A summary of previous results on the untrainability of variational quantum algorithms. A label of “✓/✗” denotes that the paper studied certain regimes where the phenomenon was present, and certain regimes where it was not. A label of “?” denotes that the phenomenon was not studied.

that for some choice of θ is the ground state of \mathbf{H} , the solution is encoded as the minimum of the loss function

$$F_{\text{VQE}}(\theta) = \langle \theta | \mathbf{H} | \theta \rangle. \quad (5)$$

This loss function can be computed on a quantum computer efficiently, particularly when \mathbf{H} has an efficient Pauli decomposition [66]. VQAs have found numerous applications [20], and a countless number of VQA instances have been proposed for various quantum learning tasks.

Typically, models in VQAs come in one of two flavors: Hamiltonian agnostic models, and Hamiltonian informed models. Hamiltonian agnostic models are constructed such that the \mathbf{U}_i are independent of \mathbf{H} , and are generally chosen to be efficient to implement. This is most analogous to the case in classical generative modeling, where the model structure is usually independent from the specific choice of data \mathbf{H} . One might hope then that training Hamiltonian agnostic VQAs is completely analogous to the classical setting, then, and the loss landscape of equation 5 exhibits the desirable properties that enable trainability found in classical networks [25, 22].

Unfortunately, unlike the classical setting, the performance of VQAs is often dominated by poor performance in the training procedure (see Appendix A for a discussion). For one, VQAs tend to exhibit *barren plateaus* when they are deep; namely, gradients of deep variational quantum circuits vanish exponentially with the problem size in many settings [60, 19, 63]. Problematic training in this regime has also been studied beyond gradient descent [21, 9].

Until recently, less was known about the trainability of VQAs in the *shallow* model regime. Numerically, [48, 79] showed that randomly chosen variational landscapes typically have poor local minima, a result which was later proven in [5] for nonlocal models using tools from random matrix theory. In a similar line of research, [81] showed that for certain quantum variational ansatzes or quantum neural networks, there exist data sets and loss functions which induce exponentially many local minima in the loss landscape. Many of these previous results on the untrainability of VQAs are summarized in Table 1, along with a summary of our results which focus on the shallow, local regime.

2.3 Quantum Statistical Query Models

Variational quantum algorithms are inherently noisy due to unavoidable sources such as the need for sampling outputs, or potentially correctable sources such as gate errors and state preparation noise. In such noisy settings, the statistical query (SQ) model provides a useful framework for quantifying the complexity of learning a class of functions by considering how many query calls to a noisy oracle are needed to learn any function in that class (see Appendix B for a brief review and history of SQ models). In the variational setting, we consider two forms of statistical queries which relate to learning a target Hamiltonian or a target unitary, both of which result in exponential hardness results for learning simple variational classes of data. For example, when aiming to learn a target Hamiltonian \mathbf{M} in our correlational quantum statistical query

model, one queries the oracle $\text{qCSQ}(\mathbf{O}, \tau)$ by inputting a bounded observable \mathbf{O} with $\|\mathbf{O}\| \leq 1$ and a tolerance τ , and the query returns a value in the range:

$$\mathbb{E}_{\rho \sim \mathcal{D}} [\text{Tr}(\mathbf{O}\rho) \text{Tr}(\mathbf{M}\rho) - \tau] \leq \text{qCSQ}(\mathbf{O}, \tau) \leq \mathbb{E}_{\rho \sim \mathcal{D}} [\text{Tr}(\mathbf{O}\rho) \text{Tr}(\mathbf{M}\rho) + \tau]. \quad (6)$$

Though the form of the above query may seem abstract, many noisy subroutines in optimization algorithms reduce to statistical queries where the tolerance τ corresponds to a “worst case” noise as we detail in Section 3.1.

Recent results have shown that certain fundamental and rather simple classes of quantum “functions” are hard to learn in the SQ setting. Namely, (classical) output distributions of locally constructed quantum states [41] and the set of Clifford circuits [37] are hard to learn given properly chosen statistical query oracles. Following these results, we show that simple classes of functions generated by variational circuits are also exponentially difficult to learn in the SQ settings we consider. Our results indicate that training algorithms must be carefully constructed to avoid these poor lower bounds.

2.4 Random Fields on Manifolds

Hardness results from barren plateaus or SQ models both intuitively arise from the exponential decay of quantities necessary to perform optimization. To analyze the shallow circuit setting beyond the SQ model—where such exponentially decaying quantities tend not to exist—we look toward models of variational loss landscapes as random fields on manifolds. This mirrors [24, 22, 5] in studying the loss landscapes of machine learning models via mapping to certain random fields which are easier to study analytically. As in [5], here we show that certain classes of variational loss functions of shallow quantum models converge in some limit to *Wishart hypertoroidal random fields* (WHRFs), for which results on the loss landscape are already known [5]. We give a brief review here.

WHRFs in q variables are random fields on a specific tensor product embedding of the hypertorus $(S^1)^{\times q}$ in \mathbb{R}^{2^q} . More specifically, points on this embedding are described by the Kronecker product:

$$\mathbf{w} = \bigotimes_{i=1}^q \begin{pmatrix} \cos(\theta_i) \\ \sin(\theta_i) \end{pmatrix} \quad (7)$$

for angles $-\pi \leq \theta_i < \pi$. These random fields are then of the form:

$$F_{\text{WHRF}}(\boldsymbol{\theta}) = \mathbf{w}^\top \cdot \mathbf{J} \cdot \mathbf{w}, \quad (8)$$

where \mathbf{J} is drawn from the normalized complex Wishart distribution $\mathcal{CW}_{2^q}(m, \boldsymbol{\Sigma})$ with m degrees of freedom. The complex Wishart distribution is a natural multivariate generalization of the gamma distribution, and is given by the distribution of the square of a complex Gaussian random matrix. Specifically, for $\mathbf{X} \in \mathbb{C}^{N \times m}$ a matrix with i.i.d. complex Gaussian columns with covariance matrix $\boldsymbol{\Sigma}$, the matrix

$$\mathbf{W} = \frac{1}{m} \mathbf{X} \cdot \mathbf{X}^\dagger \quad (9)$$

is normalized complex Wishart distributed with scale matrix $\boldsymbol{\Sigma}$ and m degrees of freedom. As discussed in [5], the loss landscapes of WHRFs exhibit a complexity phase transition governed by the *overparameterization ratio*

$$\gamma = \frac{q}{2m}, \quad (10)$$

where models with $\gamma \geq 1$ have local minima near the global minimum, and models with $\gamma \ll 1$ have local minima far from the global minimum. Thus, the degrees of freedom parameter m plays a pivotal role in governing the loss landscapes of WHRFs: when q is much smaller than m , training is typically infeasible due to an abundance of “traps” in the training landscape. Our main result in Section 4 is in demonstrating that even for certain shallow VQAs, the corresponding WHRF is such that $\gamma \ll 1$, and training is infeasible.

3 Learning in the Statistical Query Framework

In this section, we consider the hardness of learning shallow circuits in the statistical query (SQ) framework of learning theory which captures many learning algorithms used in practice [36, 45]. The SQ framework allows one to make precise statements about the complexity of learning by quantifying the number of queries one must make to a noisy oracle in order to learn a class of functions. Though this may at first appear unrelated to variational algorithms, we will show that common subroutines in optimizers for variational algorithms (e.g. obtaining gradients of variational parameters) are examples of statistical queries.

We give a brief overview of the classical SQ model here, and provide a more detailed review in Appendix B. Given an input and output space \mathcal{X} and \mathcal{Y} , let \mathcal{D} be a joint distribution on $\mathcal{X} \times \mathcal{Y}$. In the classical SQ model, one queries the SQ model by inputting a function f and receiving an estimate of $\mathbb{E}_{(x,y) \sim \mathcal{D}}[f(x, y)]$ within a given tolerance τ . As an example, one can query a loss function ℓ for a model m_{θ} with parameters θ by querying the function $\ell(m_{\theta}(x), y)$. A special class of statistical queries are inner product queries where query functions g are defined only on \mathcal{X} and the correlational statistical query returns an estimate of $\mathbb{E}_{(x,y) \sim \mathcal{D}}[g(x) \cdot y]$ within a specified tolerance τ .

In learning quantum data, observables or unitaries are the “functions” which are queried in the two settings we consider below.

Quantum correlational statistical query (qCSQ) Assume there is a target observable \mathbf{M} that we would like to learn on some distribution over states \mathcal{D} . Applying the correlational SQ model to the quantum setting, we define the query $\text{qCSQ}(\mathbf{O}, \tau)$ which takes in a bounded observable \mathbf{O} with $\|\mathbf{O}\| \leq 1$ and a tolerance τ and returns a value in the range:

$$\mathbb{E}_{\rho \sim \mathcal{D}} [\text{Tr}(\mathbf{O}\rho) \text{Tr}(\mathbf{M}\rho) - \tau] \leq \text{qCSQ}(\mathbf{O}, \tau) \leq \mathbb{E}_{\rho \sim \mathcal{D}} [\text{Tr}(\mathbf{O}\rho) \text{Tr}(\mathbf{M}\rho) + \tau]. \quad (11)$$

This setting is similar to that of [37], which showed that the class of Clifford circuits is exponentially hard to learn using statistical queries.

Quantum unitary statistical query (qUSQ) In the unitary compilation setting, one aims to learn a target unitary transformation \mathbf{U}_* over a distribution \mathcal{D} of input/output pairs of that unitary transformation. Here, the oracle $\text{qUSQ}(\mathbf{V}, \tau)$ takes in a unitary matrix \mathbf{V} and a tolerance τ and returns a value in the range:

$$\mathbb{E}_{\rho \sim \mathcal{D}} [\text{Re}[\text{Tr}(\mathbf{U}_*^\dagger \mathbf{V}\rho)] - \tau] \leq \text{qUSQ}(\mathbf{V}, \tau) \leq \mathbb{E}_{\rho \sim \mathcal{D}} [\text{Re}[\text{Tr}(\mathbf{U}_*^\dagger \mathbf{V}\rho)] + \tau]. \quad (12)$$

Importantly, if \mathcal{D} is a 1-design over n qubit states, then the above can be simplified using the formula $\mathbb{E}_{\rho \sim \mathcal{D}} [\text{Re}[\text{Tr}(\mathbf{U}_*^\dagger \mathbf{V}\rho)]] = 2^{-n} \text{Re} [\text{Tr}(\mathbf{U}_*^\dagger \mathbf{V})]$ (see proof in Lemma C.1). Queries to qUSQ are related to performing a Hadamard test [2], also a common subroutine in variational algorithms [78].

The queries above take the forms of inner products, with $\langle \mathbf{M}_1, \mathbf{M}_2 \rangle_{\mathcal{D}} = \mathbb{E}_{\rho \sim \mathcal{D}} [\text{Tr}(\mathbf{M}_1\rho) \text{Tr}(\mathbf{M}_2\rho)]$ and $\langle \mathbf{U}_1, \mathbf{U}_2 \rangle_{\mathcal{D}} = \mathbb{E}_{\rho \sim \mathcal{D}} [\text{Re} [\text{Tr}(\mathbf{U}_1^\dagger \mathbf{U}_2\rho)]]$. The inner products also induce corresponding L_2 norms: $\|\mathbf{M}\|_{\mathcal{D}} = \sqrt{\langle \mathbf{M}, \mathbf{M} \rangle_{\mathcal{D}}}$. As the magnitude of this norm can change with the dimension, we introduce the quantity C_{\max} to denote the maximum value a query can take for any target observable in the qCSQ model, i.e. $C_{\max} = \max_{\mathbf{M}: \|\mathbf{M}\| \leq 1} \|\mathbf{M}\|_{\mathcal{D}}^2$. For fair comparison, we quantify noise tolerances and hardness bounds with respect to C_{\max} . Note that for the qUSQ model $C_{\max} = 1$, but in the qCSQ model, C_{\max} can decay with the number of qubits under for example the Haar distribution of inputs.

A statistical query algorithm *learns* a function class if it can output a unitary or observable that is close to any target in that class.

Definition 3.1 (qCSQ / qUSQ learning of hypothesis class). A given algorithm using only statistical queries to qCSQ (qUSQ) successfully learns a hypothesis class \mathcal{H} consisting of observables \mathbf{M} , $\|\mathbf{M}\| \leq 1$ (unitaries \mathbf{U}) up to ϵ error if it is able to output an observable \mathbf{O} (unitary \mathbf{V}) which is ϵ -close to the unknown target observable $\mathbf{M} \in \mathcal{H}$ ($\mathbf{U} \in \mathcal{H}$) in the L_2 norm, i.e., $\|\mathbf{M} - \mathbf{O}\|_{\mathcal{D}} \leq \epsilon$ ($\|\mathbf{U} - \mathbf{V}\|_{\mathcal{D}} \leq \epsilon$).

The *statistical query dimension* quantifies the complexity of a hypothesis class \mathcal{H} and is related to the number of queries needed to learn functions drawn from a class, as summarized in Theorem 3.3.

Definition 3.2 (Statistical query dimension [13, 69]). For a distribution \mathcal{D} and concept class \mathcal{H} where $\|\mathbf{M}\|_{\mathcal{D}}^2 \leq C_{max}$ for all $\mathbf{M} \in \mathcal{H}$, the statistical query dimension (SQ-DIM $_{\mathcal{D}}(\mathcal{H})$) is the largest positive integer d such that there exists d observables $\mathbf{M}_1, \mathbf{M}_2, \dots, \mathbf{M}_d \in \mathcal{H}$ such that for all $i \neq j : |\langle \mathbf{M}_i, \mathbf{M}_j \rangle_{\mathcal{D}}| \leq C_{max}/d$.

Theorem 3.3 (Query complexity of learning [75, 13]). *Given a distribution \mathcal{D} on inputs and a hypothesis class \mathcal{H} where $\|\mathbf{M}\|_{\mathcal{D}}^2 \leq C_{max}$ for all $\mathbf{M} \in \mathcal{H}$, let $d = \text{SQ-DIM}_{\mathcal{D}}(\mathcal{H})$ be the statistical query dimension of \mathcal{H} . Any qCSQ or qUSQ learner making queries with tolerance $C_{max}\tau$ must make at least $(d\tau^2 - 1)/2$ queries to learn \mathcal{H} up to error $C_{max}\tau$.*

Since our setting differs slightly from the standard classical setting [75, 13], we include a proof of the above in Appendix C.1. For example, if the hypothesis class is rich enough to be able to express any n -qubit Pauli observable, then the statistical query dimension of that class is at least 4^n over the Haar distribution of inputs since Pauli observables are all orthogonal. This forms the basis for our resulting proofs of hardness, summarized in Table 2.

3.1 Noisy Optimization as Statistical Queries

Analogous to work in classical machine learning [36], one can perform noisy gradient descent as a series of statistical queries. As an example, consider the task of learning a target Hamiltonian \mathbf{M} by constructing a variational Hamiltonian $\mathbf{H}(\boldsymbol{\theta}) = \mathbf{U}(\boldsymbol{\theta})^\dagger \mathbf{H} \mathbf{U}(\boldsymbol{\theta})$ with parameterized Pauli rotations and minimizing the mean squared error between expectations of \mathbf{M} versus $\mathbf{H}(\boldsymbol{\theta})$ over a distribution of states \mathcal{D} . Our loss function is

$$\mathcal{L}(\boldsymbol{\theta}) = \mathbb{E}_{\rho \sim \mathcal{D}} \left[(\text{Tr}[\mathbf{M}\rho] - \text{Tr}[\mathbf{H}(\boldsymbol{\theta})\rho])^2 \right]. \quad (13)$$

By applying the parameter shift rule [70], we can evaluate the gradient of the loss with respect to parameter entry $\boldsymbol{\theta}_i$ as

$$\frac{\partial}{\partial \boldsymbol{\theta}_i} \mathcal{L}(\boldsymbol{\theta}) = \mathbb{E}_{\rho \sim \mathcal{D}} \left[\left(\text{Tr}[\mathbf{H}(\boldsymbol{\theta})\rho] - \text{Tr}[\mathbf{M}\rho] \right) \left(\text{Tr}[\mathbf{H}(\boldsymbol{\theta}^+)\rho] - \text{Tr}[\mathbf{H}(\boldsymbol{\theta}^-)\rho] \right) \right], \quad (14)$$

where $\boldsymbol{\theta}^+$ and $\boldsymbol{\theta}^-$ are the values of the parameters shifted at the i -th entry according to the parameter shift rule for the gradient. The quantity $\mathbb{E}_{\rho \sim \mathcal{D}} [\text{Tr}[\mathbf{H}(\boldsymbol{\theta})\rho](\text{Tr}[\mathbf{H}(\boldsymbol{\theta}^+)\rho] - \text{Tr}[\mathbf{H}(\boldsymbol{\theta}^-)\rho])]$ can be directly evaluated without statistical queries, and the quantity $\mathbb{E}_{\rho \sim \mathcal{D}} [\text{Tr}[\mathbf{M}\rho](\text{Tr}[\mathbf{H}(\boldsymbol{\theta}^+)\rho] - \text{Tr}[\mathbf{H}(\boldsymbol{\theta}^-)\rho])]$ can be evaluated using 2 statistical queries to qCSQ where the tolerance τ accounts for the noise in the estimate.

As a second example, this time in the unitary compiling setting of qUSQ, we can evaluate the commonly used procedure of measuring the inner product or average fidelity of n -qubit states between a target unitary \mathbf{U}_* and a variationally chosen unitary $\mathbf{V}(\boldsymbol{\theta})$ using statistical queries analogous to a swap test on actual quantum hardware [61, 16, 46, 12]. With slight abuse of notation, let $|\phi\rangle \sim \mathcal{D}$ denote a distribution over pure states which forms a 2-design. Then by application of Lemma C.12 the average fidelity equals

$$\mathbb{E}_{|\phi\rangle \sim \mathcal{D}} \left[F(\mathbf{U}_*|\phi\rangle, \mathbf{V}(\boldsymbol{\theta})|\phi\rangle) \right] = \mathbb{E}_{|\phi\rangle \sim \mathcal{D}} [|\langle \phi | \mathbf{V}(\boldsymbol{\theta})^\dagger \mathbf{U}_* | \phi \rangle|^2] = \frac{2^{-n} |\text{Tr}(\mathbf{V}(\boldsymbol{\theta})^\dagger \mathbf{U}_*)|^2 + 1}{2^n + 1}. \quad (15)$$

Note, that the key quantity $|\text{Tr}(\mathbf{V}(\boldsymbol{\theta})^\dagger \mathbf{U}_*)|^2 = \text{Re}[\text{Tr}(\mathbf{V}(\boldsymbol{\theta})^\dagger \mathbf{U}_*)]^2 + \text{Re}[i \text{Tr}(\mathbf{V}(\boldsymbol{\theta})^\dagger \mathbf{U}_*)]^2$ can be evaluated up to a desired tolerance using statistical queries qUSQ($\mathbf{V}(\boldsymbol{\theta}), \tau$) and qUSQ($i\mathbf{V}(\boldsymbol{\theta}), \tau$). As before, the tolerance τ in the queries accounts for the noise in the estimation of the quantity above.

One important caveat must be noted that in the SQ setting, learning must succeed for all values of the query within the given tolerance τ . Noise in quantum settings, which can arise from sampling a finite data set, gate error, state preparation error, measurement sampling noise, or other means does not exactly coincide with the assumed tolerance of an SQ model. Nevertheless, though noise during optimization may appear unnatural in classical settings, such noise in quantum settings is rather endemic and the SQ model allows one to rigorously analyze the complexity of learning in a worst case noise model.

3.2 Hardness of SQ Learning Variational Function Classes

SQ	Setting (n qubits, L layers)	Query Complexity ($\beta < 1/2^*$)	Proof
qCSQ	$L = 1$, global measurement, single qubit gates	$2^{\Omega(n)}$ if $\tau \geq 3^{-\beta n}$	Corollary C.3
qCSQ	$L = \lceil \log_2 n \rceil$, single qubit measurement, global 2-local gates	$2^{\Omega(n)}$ if $\tau \geq 4^{-\beta n}$	Corollary C.5
qCSQ	$L \ll n$, single qubit measurement, neighboring 2-local gates on d -dim. lattice	$2^{\Omega(L^d)}$ if $\tau = \Omega(1)^{**}$	Corollary C.9
qUSQ	$L = 1$, single qubit gates	$2^{\Omega(n)}$ if $\tau \geq 4^{-\beta n}$	Corollary C.11

* Technically, we require $\beta = 1/2 - \Omega(1)$; ** $\tau = 2^{\omega(\min(2L, n^{1/d})^d)}$ is sufficient.

Table 2: Relatively simple classes of functions require exponentially many statistical queries to learn using any naive algorithm that reduces to statistical queries. The table above quantifies the number of queries needed to identify a target function in the function class, over a distribution of states that forms a 2-design and with queries that have tolerance $C_{max}\tau$ (query tolerance lower bounded by a constant times C_{max} suffices in all cases).

To quantify the hardness of learning variational circuits, we consider the task of learning certain function classes generated by shallow variational circuits over a distribution of inputs \mathcal{D} which forms a 2-design. As an aside, for the qCSQ setting, our results also generally hold for distributions that are uniform over states in the computational basis, recovering the statistical query setting for classical Boolean functions. Table 2 summarizes the number of queries needed to learn various function classes which are generated by variational circuits. In either the qCSQ or qUSQ setting, an exponential number of queries (in either n or the light cone size) are needed to learn simple classes, such as the class of functions generated by single qubit gates followed by a fixed global measurement. This hardness intuitively arises because each individual query can only obtain information about a few of the exponentially many orthogonal elements in the statistical query dimension.

These results do not indicate that simple classes of functions like those generated by single qubit rotations are hard to learn for *any* algorithm, but only those whose steps reduce to statistical queries. For example, the class of Pauli channels is not learnable in the SQ setting, but there exist simple, carefully constructed, algorithms which can learn Pauli channels [23, 43, 37]. This is analogous to the classical setting where parity functions are hard to learn in the noisy SQ setting, but efficient to learn using simple linear regression [45]. Similarly, the related work of [41] showed that output distributions of Clifford circuits can be hard to learn using statistical queries, but efficient using a technique that resorts to linear regression on a matrix formed from samples of the overall distribution. More loosely, our results provide support to the basic maxim that algorithms which apply too broadly will work very rarely [80]. One straightforward way to avoid the hardness of the SQ setting is to construct algorithms whose basic steps do not reduce to statistical queries, e.g. via the construction of non-global metrics [47, 42, 46]. However, such a fix is by no means guaranteed to avoid the more general issues of poor landscapes and noise that also make learning in the SQ setting so difficult, as we examine next.

4 Loss Landscapes of Shallow Variational Quantum Algorithms

4.1 Shallow VQAs as WHRFs

We now move on to discussing the trainability of variational quantum algorithms (VQAs) in another light. Namely, are the *loss landscapes* of shallow, local VQAs with Hamiltonian agnostic ansatzes amenable to optimization? As discussed in Section 2.2, it is already known that deep Hamiltonian agnostic ansatzes are typically untrainable due to the presence of barren plateaus [60, 19, 63]; hence, here we focus on shallow ansatzes. Previous results [5] have also shown that shallow, *nonlocal* models exhibit poor local minima. We extend these latter results to certain *local models*, using similar techniques: we show that the loss landscapes

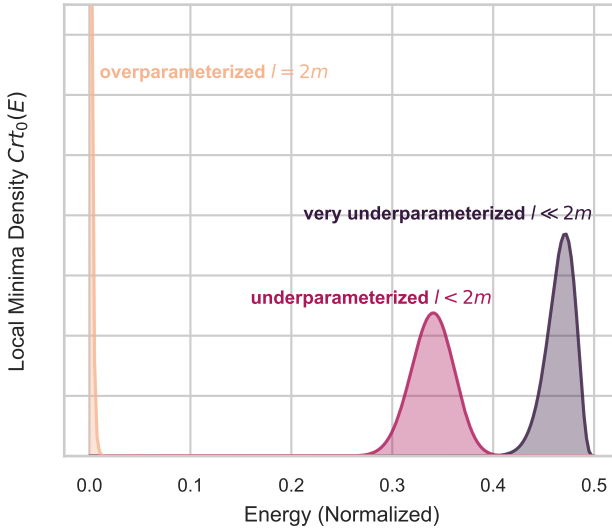


Figure 2: Plot of the asymptotic distribution of local minima of WHRFs with m degrees of freedom on the l -torus in: the extremely underparameterized regime, where $l \ll 2m$; the moderately underparameterized regime, where l is a finite fraction of $2m$; and at the critical overparameterization regime, where $l = 2m$. Here, the energy is scaled and shifted as per equation 19 so that global minima have zero energy. In the underparameterized regime, only a fraction $\sim \exp(-m)$ of the critical points are within any constant additive error of the global minimum. In the overparameterized regime, local minima are exponentially concentrated at the global minimum.

of certain shallow, local VQAs are close to those of Wishart hypertoroidal random fields (WHRFs; see Section 2.4 for a brief review). As we proceed in this Section, we will therefore use various properties of the critical point distributions of WHRFs, which are due to [5].

The loss landscapes of WHRFs are known to exhibit a computational phase transition, governed by the order parameter

$$\gamma = \frac{l}{2m}, \quad (16)$$

called the *overparameterization ratio*. Here, l is the number of parameters of the WHRF, and m its degrees of freedom (see Section 2.4). When $\gamma \ll 1$ (the *underparameterized regime*), WHRFs exhibit poor local minima and thus are essentially untrainable; when $\gamma \geq 1$ (the *overparameterized regime*), however, essentially all local minima of a WHRF are close to the global minimum in function value. The asymptotic expression of the distribution of local minima is also known, which is given by (up to a normalization factor):

$$Crt_0(E) \sim e^{-mE} E^{m-l/2} (1-2E)^l \quad (17)$$

for the density of local minima at any given energy $0 \leq E \leq \frac{1}{2}$, in units of the mean eigenvalue of \mathbf{H} (shifted such that the global minimum is at $E = 0$). Representative plots of this distribution in various regimes are shown in Figure 2.

We now summarize our results, discussed in more technical details in Appendix D. To begin, we take our (assumed traceless) problem Hamiltonian to have Pauli decomposition:

$$\mathbf{H} = \sum_{i=1}^A \alpha_i \mathbf{P}_i, \quad (18)$$

and for simplicity scale and shift the loss landscape of equation 5 to be of the form:

$$F_{\text{VQE}}(\boldsymbol{\theta}) = 1 + \|\boldsymbol{\alpha}\|_1^{-1} \sum_{i=1}^A \alpha_i \langle \boldsymbol{\theta} | \mathbf{P}_i | \boldsymbol{\theta} \rangle, \quad (19)$$

where $\boldsymbol{\alpha}$ is the vector of all α_i and the ansatz $|\boldsymbol{\theta}\rangle$ is as given in equation 4. As this ansatz is assumed to be shallow and local, we assume that the reverse light cone of each \mathbf{P}_i under the ansatz is of size $l \ll n$.

As in most analytic treatments of Hamiltonian agnostic VQAs, we consider certain randomized classes of ansatzes [60, 19, 63, 5]. Previous results on the loss landscape of nonlocal VQAs [5] considered models that *globally* scrambled. Our results here weaken this assumption, only assuming that *locally* the ansatz scrambles. Roughly, we assume that in a local region around each measured Pauli observable \mathbf{P}_i , the ansatz is an ϵ -approximate t -design; that is, roughly, its first t moments are ϵ -close to those of the Haar distribution. This is a much weaker assumption than global scrambling. For instance, for \mathbf{P}_i of constant weight, such distributions are naturally sampled from constant depth local circuits with random local gates [40]. We discuss in more detail when this assumption holds in practice in Section 4.2, and defer technical details to Appendix D.

Our main result, informally, is that the random field given by equation 19 under this local scrambling assumption converges in distribution to that of a WHRF. The formal statement and derivation of this result are given in Appendix D, where we also lay out our assumptions more explicitly.

Theorem 4.1 (Approximately locally scrambled variational loss functions converge to WHRFs, informal). *Let*

$$m \equiv \frac{\|\boldsymbol{\alpha}\|_1^2}{\|\boldsymbol{\alpha}\|_2^2} 2^{l-1} \quad (20)$$

be the degrees of freedom parameter. Assume $q \log(q) = o(m)$, where q is the number of ansatz parameters in the reverse light cone of each \mathbf{P}_i . Then, the distribution of variational loss functions of the form of equation 19 is equal to that of a WHRF

$$F_{\text{WHRF}}(\boldsymbol{\theta}) = m^{-1} \sum_{i,j=1}^{2^l} w_i J_{i,j} w_j \quad (21)$$

with m degrees of freedom, up to an error in distribution on the order of $\tilde{O}(\text{poly}(\frac{1}{t} + \epsilon + \exp(-l)))$. Here, w are points on the hypertorus $(S^1)^{\times l}$ parameterized by $\tilde{\boldsymbol{\theta}}$, where $\tilde{\theta}_i$ is the sum of all θ_j on qubit i .

We interpret this result as the degrees of freedom m of the model being given by roughly the sum of the *local* Hilbert space dimensions of the reverse light cones of terms in the Pauli decomposition of \mathbf{H} . Note that the degrees of freedom parameter m of the WHRF given by equation 21 is typically polynomial in n (in the shallow ansatz regime, where $l = O(\log(n))$). In particular, it is easy to see from [5] that these WHRFs suffer from no barren plateaus. However, as typically $l \ll m$, these models still exhibit poor distributions of local minima; we interpret this as the *local underparameterization* of the model, to be contrasted with the *global underparameterization* interpretation when m is exponentially large in n .

More specifically, WHRFs have a superpolynomially small (in n) fraction of local minima within any given constant δ of the global minimum when

$$\gamma = \frac{\|\boldsymbol{\alpha}\|_2^2 l}{\|\boldsymbol{\alpha}\|_1^2 2^l} = o\left(\frac{1}{\log(n)}\right). \quad (22)$$

Assuming all $\alpha_i = \Theta(1)$ —and taking into account the assumption on $q \log(q)$ from Theorem 4.1—we thus expect poor optimization performance when:

$$2^l A \gg l \log(n) + q \log(q). \quad (23)$$

Interesting cases—assuming the number of ansatz parameters in each reverse light cone $q = O(\text{poly}(l))$ —include when the number of qubits in each reverse light cone is logarithmic in n (i.e. $l = \Theta(\log(n))$), or when the number of terms in the Pauli decomposition grows linearly in n while the size of the reverse light cones is at most logarithmic in n (i.e. $A = \Omega(n)$ and $l = O(\log(n))$). These include instances where barren plateaus are not expected to occur [63].

4.2 Classes of Shallow Ansatzes with Poor Local Minima

As we have previously mentioned, our results rely on the *local approximate scrambling* of the given variational ansatz. We now informally discuss various classes of shallow ansatzes, and how our results apply to them.

Checkerboard ansatzes First, let us consider d -dimensional checkerboard ansatzes of constant depth. Fix p, t to be sufficiently large constants. We assume that the initial state forms an $O\left(\frac{1}{\text{poly}(t)}\right)$ -approximate t design on l qubits around each Pauli observable of weight k ; this can be done via a depth p , d -dimensional circuit of 2-local Haar random unitaries when $l = O\left(\frac{(p+k)^d}{\text{poly}(t)}\right) \geq k$ for some fixed polynomial in t [40, 39].

After this state preparation circuit, a traditional depth $\Theta\left(l^{\frac{1}{d}}\right)$ (i.e. independent of n), d -dimensional, n qubit checkerboard circuit is applied, with observable reverse light cones of size at greatest l . By the discussion in Section 4.1 and Appendix D, these variational ansatzes are untrainable due to poor local minima, yet by the results of [63] do not suffer from barren plateaus.

One interesting consideration is extending this result to “traditional” checkerboard ansatzes, without the special state preparation procedure we have considered. There, the $l = O\left(\frac{(p+k)^d}{\text{poly}(t)}\right)$ qubit local state is mixed, and our results therefore do not directly apply. However, we expect no reason for the mixedness of the initial state to improve training performance in any way. We validate this intuition numerically in Section 5.

Quantum convolutional neural networks We also consider a class of models similar to quantum convolutional neural networks (QCNNs) [28] previously shown not to suffer from barren plateaus [67]. Though these models are in full generality trained on arbitrary loss functions, for learning various physical models the loss may take the form of equation 5. QCNNs are defined by their measurement of a subset of qubits at periodic intervals, via so-called *pooling layers*; for sufficiently deep (i.e. large constant depth) convolutional layers, then, at some point in the model, the number of remaining qubits will be sufficiently small such that the remaining convolutional layers are approximately scrambling. If one then assumes that the initial states are adversarially chosen such that they remain pure by this layer, this scenario reduces to the shallow checkerboard ansatz scenario, and once again we expect poor local minima by Theorem 4.1. Even if the initial states are not adversarially chosen and the input to the scrambling convolutional layers is mixed, we expect by similar intuition the model to remain untrainable; we see this numerically, for instance, in Section 5.1. We also see in Section 5.1 that this poor training occurs even when training on loss functions beyond equation 5.

5 Numerical Results

To numerically validate our results on the hardness of learnability in variational settings, we perform numerical simulations showing that learning in various settings cannot be guaranteed unless exponentially many parameters are included in an ansatz. We only consider problems and ansatzes where the existence of a zero loss global minima is guaranteed for even a shallow instance of the ansatz to study whether or not optimizers can actually find the global minimum or a similarly good critical point. We parameterize all trainable 2-qubit gates in the Lie algebra of the 4-dimensional unitary group, and implement the resulting unitary matrix via the exponential map which is surjective and capable of expressing any local 4×4 unitary gate. In all cases, we perform simulations using calculations with computer precision and analytic forms of the gradient (see

Appendix E for more details). In practice, actual quantum implementations will be hampered by various sources of inefficiency such as the lack of an analogous method of backpropagation for calculating gradients, sampling noise, or even gate errors. Thus, our numerical analysis can be interpreted as a “best case” setting for quantum computation where we disregard such inefficiencies and focus solely on learnability.¹

5.1 Teacher-Student Learning

One may conjecture that it is plausible to learn the class of functions generated by relatively shallow depth variational circuits by parameterizing a shallow-depth circuit of the same form and training its parameters. In this “teacher-student” setup where a student circuit aims to learn a randomized teacher circuit, one may assume that learnability is in fact efficient and possible. Unlike many problems in quantum chemistry and VQE, we are guaranteed here to have the existence of a “perfect” global minimum since recovering the parameters of the teacher circuit achieves zero loss. Nevertheless, we showed earlier that such circuits are likely to have many poor local minima and are hard to learn in the statistical query setting. Here, we provide numerical evidence of these findings.

Quantum convolutional neural network The quantum convolutional neural network (QCNN) presents an interesting test bed for our analysis since it has been shown in prior work to avoid barren plateaus [67]. However, as we will show numerically, the QCNN, like other models, is riddled with poor local minima in generic learning tasks. For our analysis, we attempt to learn randomly generated quantum convolutional neural networks (QCNNs) denoted as the teacher circuit, with a parameterized QCNN of the same form denoted as the student circuit. In the QCNN, both student and teacher circuits have parameterized 2-qubit gates at each layer, and 2-qubit pooling occurs after a convolutional layer. Each 2-qubit gate is fully parameterized in the Lie algebra of the unitary group. Networks are trained to predict the probability of the measurement of the last qubit in the teacher circuit. We measure the performance via the classification accuracy, where a prediction is considered correct when it predicts the most likely measurement of the last qubit correctly. Networks are trained via the Adam optimizer [52] to learn outputs of 512 randomly chosen computational basis states. QCNNs with 4, 8, 12, and 16 qubits have 32, 48, 64, and 64 trainable parameters, respectively.

Figure 3 plots the final training accuracy achieved over 100 random simulations for varying ranges of circuit sizes. For circuits with 4 qubits, the training is sometimes successful, often achieving an accuracy above 85 percent on the training dataset. However, as the number of qubits grows, even past 8 qubits, the optimizer is unable to recover parameters which match the outputs of the teacher circuit. The results here show that the QCNN circuit—which has $O(\log n)$ depth—still scrambles outputs to hinder learnability.

Checkerboard ansatz One particular challenge with quantum variational learning, in contrast to classical machine learning, is that exponential resources are needed to overparameterize a model. In quantum settings, to be able to reduce the training loss arbitrarily well, overparameterization is typically needed with respect to the dimension of the quantum input state (the Hilbert space dimension), whereas classically, overparameterization with respect to the size of the data set typically suffices [24, 56, 8]. To illustrate this phenomenon, we consider learning states generated by random shallow checkerboard circuits (denoted the teacher circuit) using checkerboard circuits of the same or more depth (denoted the student circuit). The data set used to train the circuit consist of 512 pairs of inputs randomly drawn from computational basis states with their corresponding output state taken from applying the input state to the teacher circuit. We use the loss $\ell(|\psi\rangle, |\phi\rangle) = 1 - |\langle\psi|\phi\rangle|^2$ to measure the success of learning. Note that, though this is a global loss metric, gradients are analytically calculated to precision sufficient enough to obtain accurate values of the gradients for the relatively small number of qubits considered here.

As shown in Figure 4, exponential depth (and number of parameters) is needed to always successfully learn the data generated by a shallow checkerboard circuit of 4 layers. Since overparameterizing a model requires exponentially many parameters, we considered ansatzes only over 8 qubits, which is small enough to

¹Code is available at this repository: <https://github.com/bkiani/Beyond-Barren-Plateaus>

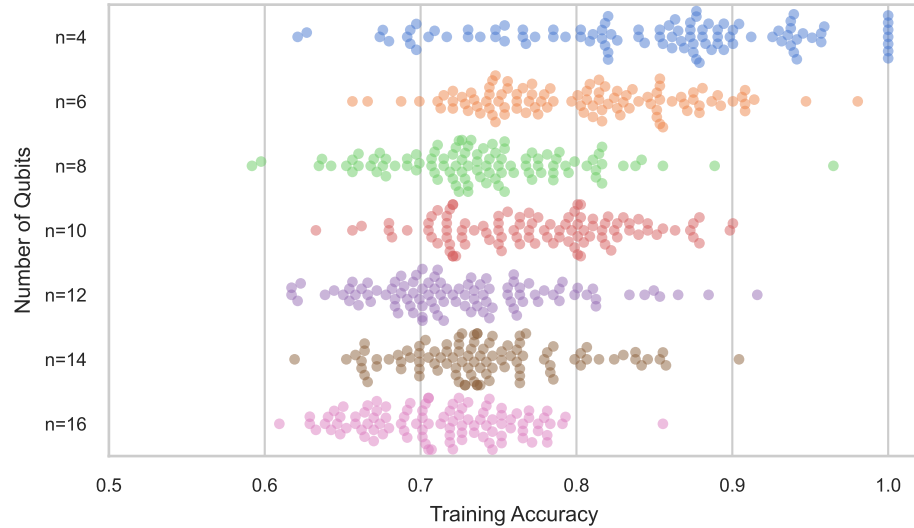


Figure 3: **QCNN**: The student circuit is unable to learn the teacher circuit as the number of qubits grows, converging to a local minimum of the loss landscape. The existence of a global optimum is guaranteed as the teacher circuit is drawn from a random initialization of the same QCNN structure of the student circuit. Here, for a ranging number of qubits, 100 student circuits are trained to learn randomized teacher circuits of the same form and the resulting swarm plots of the final training accuracy are shown.

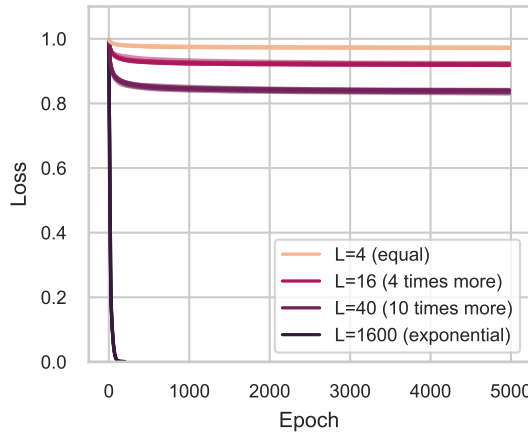


Figure 4: **Checkerboard**: Exponential depth is needed to overparameterize a model to successfully learn a random circuit of the same form. Here, for each depth of the student denoted by L , 10 randomly initialized 8 qubit student circuits are trained to learn a random 4 layer teacher circuit drawn from the same ansatz and parameter distribution.

be able to feasibly overparameterize the models in our simulations. For fewer qubits and shallower circuits, we found that learning with equal numbers of qubits and layers was sometimes successful; but unsurprisingly, as we show in Section 5.2, learning becomes much harder as qubits are added.

5.2 Variational Quantum Eigensolvers

In our VQE simulations, we consider problems and ansatzes which are capable of recovering the global minimum to study whether or not VQE converges to a poor local minimum during optimization. We aim to find the ground states of local Hamiltonians \mathbf{H}_t over n qubits that take the form of a sum of single qubit Pauli \mathbf{Z} Hamiltonians, conjugated by L layers of two alternating unitary operators \mathbf{U}_1 and \mathbf{U}_2 which are product unitaries on neighboring 2-local qubits:

$$\mathbf{H}_t = (\mathbf{U}_2^\dagger \mathbf{U}_1^\dagger)^L \left[\sum_{i=1}^n \mathbf{Z}_i \right] (\mathbf{U}_1 \mathbf{U}_2)^L + n\mathbf{I}. \quad (24)$$

The added identity matrix normalizes the Hamiltonian so that the ground state has energy 0. Since the ground state of $\sum_{i=1}^n \mathbf{Z}_i$ is the state $|1\rangle^{\otimes n}$, we are guaranteed the existence of a global minima when using a checkerboard ansatz of at least depth L , since this ansatz can “undo” the conjugation by the unitary operators.

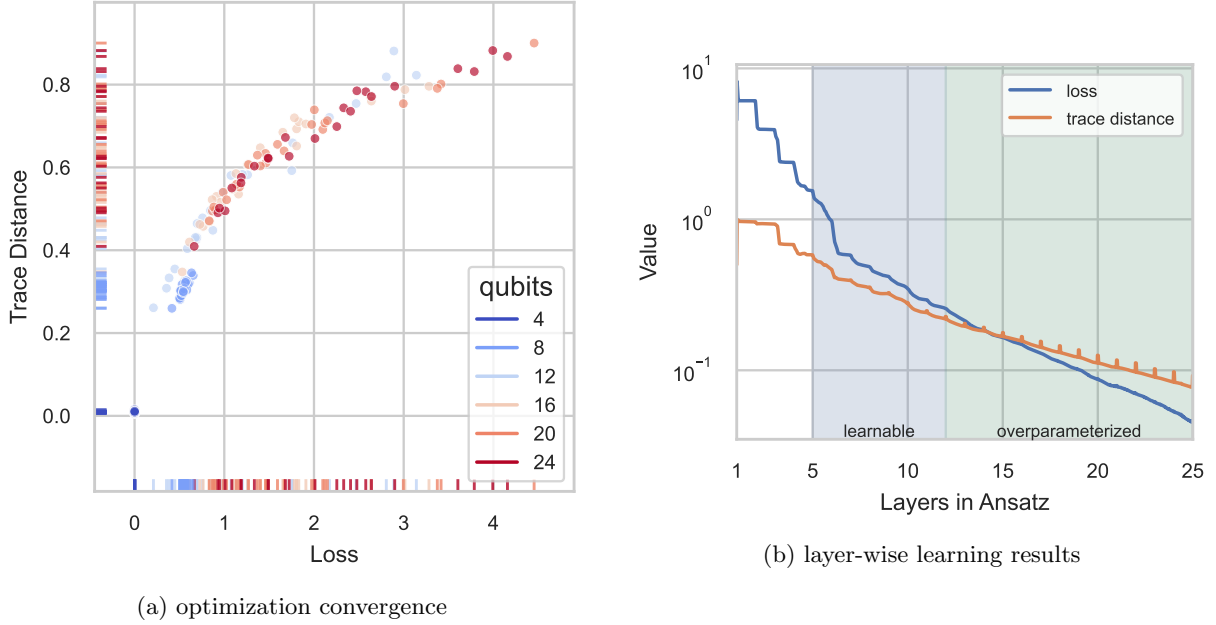


Figure 5: **VQE:** (a) Scatter plot of the final loss and trace distance of the VQE state after 30000 steps of gradient descent optimization shows that the algorithm converges to poorer local minima as the number of qubits grows. 24 simulations are performed for each value of n . The algorithm always succeeds at obtaining the ground state with 4 qubits, but progressively struggles more with added qubits. (b) When optimizing in a layer-wise fashion, VQE algorithm converges to a local minimum at each layer until the overparameterized regime where the loss function steadily decreases regardless of the number of layers. Even in the learnable regime where the checkerboard ansatz is capable of expressing the global minima, the ansatz is still unable to find the correct parameters for this global minimum. Bumps in the loss function appear due to small instabilities in training immediately after adding a layer.

We measure the performance of optimization by considering two different metrics. The first metric is the loss function itself, which is the average value of the energy $\langle \psi | \mathbf{H}_t | \psi \rangle$ of the VQE ansatz state $|\psi\rangle$ for the given Hamiltonian \mathbf{H}_t . The second metric is the trace distance to the ground state $|\phi_g\rangle$ of \mathbf{H}_t , equal to $\| |\phi_g\rangle \langle \phi_g| - |\psi\rangle \langle \psi| \|_1/2$. If the VQE optimization converges to the ground state, both of these metrics are equal to zero.

We first aim to learn the target Hamiltonian \mathbf{H}_t using a checkerboard ansatz with $L = 4$ layers, equal in depth to the Hamiltonian conjugation circuit and thus capable of recovering the ground state. In Figure 5a, we plot the final values of the loss and trace distance for 24 randomly initialized VQE problems for a number of qubits ranging from 4 to 24. Here, we perform optimization using vanilla gradient descent to explore the distribution of local minima in the landscape. Similar results are observed when using more advanced optimizers such as Adam (see Appendix E.3). As evident in the plot and consistent with our theoretical findings, convergence clusters around local minima far from the ground state, particularly as the number of qubits grows. In Figure 5b, we train an 11 qubit ansatz using a layer-wise optimizer [73, 38], which initially trains a single layer of the ansatz and adds layers after every 5000 steps to continually add expressiveness. The target Hamiltonian \mathbf{H}_t here has 4 layers of perturbations applied to it. Although layer-wise optimizers can avoid issues with barren plateaus [73], our numerical findings clearly show that this does not guarantee the algorithm will avoid traps in the landscape. After 5 layers, the ansatz has enough parameters to capably express the global optimum (denoted by the label “learnable”), but nevertheless stalls in optimizing to the ground state. Not until there are at least 12 layers, enough to overparameterize the ansatz with respect to the Hilbert space dimension, does learning smoothly converge to the globally optimal solution.

6 Conclusion

Though variational quantum algorithms—and quantum machine learning models in general—have been cited as perhaps the most promising use case for quantum devices in the near future [68], theoretical guarantees of their performance have been sparse. Here, we have excluded a wide class of variational algorithms by showing that typically, they are in fact *not* trainable. We showed this in two different frameworks: first, in Section 3, we studied various classes of quantum models in the statistical query framework. We showed that under worst case noise, typically exponentially many queries in the problem size are needed for these models to learn. As a complementary approach, we also examined the typical loss landscapes of variational quantum algorithms in Section 4, and showed that even at constant depth these models can have a number of poor local minima exponentially large in the problem size. We also numerically confirmed these results for a variety of problems in Section 5. These results go beyond the typical studies on the presence of barren plateaus, as these models have gradients vanishing only polynomially quickly in the problem size. Our work demonstrates that showing that barren plateaus are not present in a model does not necessarily vindicate it as trainable. We also discuss in Appendix F how our results apply beyond typical gradient descent-based optimizers.

These results, though they exclude a wide variety of variational quantum algorithms, still leave room for hope in the usefulness of these algorithms. Particularly, our analysis focuses on very general, Hamiltonian agnostic ansatzes; in various instances, more focused ansatzes may be trainable. For instance, as previously shown in [34], for certain classes of problems the quantum approximate optimization algorithm (QAOA) [33] is provably able to outperform the best unconditionally proven classical algorithms, even when taking into account the training of the model. Even in the Hamiltonian agnostic regime, one may be interested in studying a system with some unknown symmetries, greatly reducing the effective degrees of freedom of the ansatz itself. Though we prove no such result directly, intuitively our results stem from the underparameterization of the quantum ansatz. Highly symmetric models may be immanently more trainable due to this fact. Similar phenomena were studied in [53]. We discuss these and other potentially trainable regimes in more detail in Appendix G.

Our results contribute to the already vast library of literature on the trainability of variational quantum models in further culling the landscape of potentially trainable quantum models. We hope these results have the effect of focusing research efforts toward classes of models that have the potential for trainability, and whittle down the search for practical use cases of variational quantum algorithms.

Acknowledgments

The authors thank Giacomo De Palma, Seth Lloyd, Milad Marvian, Quynh T. Nguyen, and Agnes Villanyi for helpful feedback and discussions. E.R.A. is supported by the National Science Foundation Graduate Research Fellowship Program under Grant No. 4000063445.

References

- [1] Dorit Aharonov, Jordan Cotler, and Xiao-Liang Qi. Quantum algorithmic measurement. *Nature communications*, 13(1):1–9, 2022.
- [2] Dorit Aharonov, Vaughan Jones, and Zeph Landau. A polynomial quantum algorithm for approximating the Jones polynomial. *Algorithmica*, 55(3):395–421, 2009.
- [3] Mohammad H. Amin, Evgeny Andriyash, Jason Rolfe, Bohdan Kulchytskyy, and Roger Melko. Quantum boltzmann machine. *Phys. Rev. X*, 8:021050, 5 2018.
- [4] Eric R. Anschuetz and Yudong Cao. Realizing quantum boltzmann machines through eigenstate thermalization, 2019.
- [5] Eric Ricardo Anschuetz. Critical points in quantum generative models. In *International Conference on Learning Representations*, 2022.
- [6] Anurag Anshu, Srinivasan Arunachalam, Tomotaka Kuwahara, and Mehdi Soleimanifar. Sample-efficient learning of interacting quantum systems. *Nat. Phys.*, 17(8):931–935, 2021.
- [7] Benny Applebaum, Boaz Barak, and David Xiao. On basing lower-bounds for learning on worst-case assumptions. In *2008 49th Annual IEEE Symposium on Foundations of Computer Science*, pages 211–220. IEEE, 2008.
- [8] Sanjeev Arora, Simon S Du, Wei Hu, Zhiyuan Li, Russ R Salakhutdinov, and Ruosong Wang. On exact computation with an infinitely wide neural net. *Advances in Neural Information Processing Systems*, 32, 2019.
- [9] Andrew Arrasmith, M Cerezo, Piotr Czarnik, Lukasz Cincio, and Patrick J Coles. Effect of barren plateaus on gradient-free optimization. *Quantum*, 5:558, 2021.
- [10] Srinivasan Arunachalam, Alex B Grilo, and Henry Yuen. Quantum statistical query learning. *arXiv preprint arXiv:2002.08240*, 2020.
- [11] Leonardo Banchi, Jason Pereira, and Stefano Pirandola. Generalization in quantum machine learning: A quantum information standpoint. *PRX Quantum*, 2(4):040321, 2021.
- [12] Kerstin Beer, Dmytro Bondarenko, Terry Farrelly, Tobias J Osborne, Robert Salzmann, Daniel Scheiermann, and Ramona Wolf. Training deep quantum neural networks. *Nature communications*, 11(1):1–6, 2020.
- [13] Avrim Blum, Merrick Furst, Jeffrey Jackson, Michael Kearns, Yishay Mansour, and Steven Rudich. Weakly learning dnf and characterizing statistical query learning using fourier analysis. In *Proceedings of the twenty-sixth annual ACM symposium on Theory of computing*, pages 253–262, 1994.
- [14] Léon Bottou and Olivier Bousquet. The tradeoffs of large-scale learning. *Optimization for machine learning*, page 351, 2011.
- [15] Fernando G. S. L. Brandao, Michael Broughton, Edward Farhi, Sam Gutmann, and Hartmut Neven. For fixed control parameters the quantum approximate optimization algorithm’s objective function value concentrates for typical instances, 2018.

- [16] Harry Buhrman, Richard Cleve, John Watrous, and Ronald De Wolf. Quantum fingerprinting. *Physical Review Letters*, 87(16):167902, 2001.
- [17] Ernesto Campos, Aly Nasrallah, and Jacob Biamonte. Abrupt transitions in variational quantum circuit training. *Physical Review A*, 103(3):032607, 2021.
- [18] Matthias C Caro, Hsin-Yuan Huang, M Cerezo, Kunal Sharma, Andrew Sornborger, Lukasz Cincio, and Patrick J Coles. Generalization in quantum machine learning from few training data. *arXiv preprint arXiv:2111.05292*, 2021.
- [19] M. Cerezo, Akira Sone, Tyler Volkoff, Lukasz Cincio, and Patrick J. Coles. Cost function dependent barren plateaus in shallow parametrized quantum circuits. *Nat. Commun.*, 12(1):1791, 2021.
- [20] Marco Cerezo, Andrew Arrasmith, Ryan Babbush, Simon C Benjamin, Suguru Endo, Keisuke Fujii, Jarrod R McClean, Kosuke Mitarai, Xiao Yuan, Lukasz Cincio, et al. Variational quantum algorithms. *Nature Reviews Physics*, 3(9):625–644, 2021.
- [21] Marco Cerezo and Patrick J Coles. Impact of barren plateaus on the hessian and higher order derivatives. *arXiv e-prints*, pages arXiv–2008, 2020.
- [22] Pratik Chaudhari and Stefano Soatto. On the energy landscape of deep networks, 2017.
- [23] Senrui Chen, Sisi Zhou, Alireza Seif, and Liang Jiang. Quantum advantages for pauli channel estimation. *Physical Review A*, 105(3):032435, 2022.
- [24] Anna Choromanska, Mikael Henaff, Michael Mathieu, Gérard Ben Arous, and Yann LeCun. The loss surfaces of multilayer networks. In *Artificial intelligence and statistics*, pages 192–204. PMLR, 2015.
- [25] Anna Choromanska, Mikael Henaff, Michael Mathieu, Gerard Ben Arous, and Yann LeCun. The Loss Surfaces of Multilayer Networks. In Guy Lebanon and S. V. N. Vishwanathan, editors, *Proceedings of the Eighteenth International Conference on Artificial Intelligence and Statistics*, volume 38 of *Proceedings of Machine Learning Research*, pages 192–204, San Diego, California, USA, 5 2015. PMLR.
- [26] Benoît Collins. Moments and cumulants of polynomial random variables on unitarygroups, the itzykson-zuber integral, and free probability. *International Mathematics Research Notices*, 2003(17):953–982, 2003.
- [27] Benoît Collins and Piotr Śniady. Integration with respect to the haar measure on unitary, orthogonal and symplectic group. *Communications in Mathematical Physics*, 264(3):773–795, 2006.
- [28] Iris Cong, Soonwon Choi, and Mikhail D. Lukin. Quantum convolutional neural networks. *Nat. Phys.*, 15(12):1273–1278, 8 2019.
- [29] Giacomo De Palma, Milad Marvian, Dario Trevisan, and Seth Lloyd. The quantum wasserstein distance of order 1. *IEEE Trans. Inf. Theory*, 67(10):6627–6643, 2021.
- [30] Ilias Diakonikolas, Daniel M Kane, Vasilis Kontonis, and Nikos Zarifis. Algorithms and sq lower bounds for pac learning one-hidden-layer relu networks. In *Conference on Learning Theory*, pages 1514–1539. PMLR, 2020.
- [31] Yuxuan Du, Min-Hsiu Hsieh, Tongliang Liu, and Dacheng Tao. Expressive power of parametrized quantum circuits. *Physical Review Research*, 2(3):033125, 2020.
- [32] Yuxuan Du, Zhuozhuo Tu, Xiao Yuan, and Dacheng Tao. Efficient measure for the expressivity of variational quantum algorithms. *Physical Review Letters*, 128(8):080506, 2022.
- [33] Edward Farhi, Jeffrey Goldstone, and Sam Gutmann. A quantum approximate optimization algorithm, 2014.

[34] Edward Farhi, Jeffrey Goldstone, Sam Gutmann, and Leo Zhou. The quantum approximate optimization algorithm and the Sherrington–Kirkpatrick model at infinite size, 2019.

[35] Xun Gao, Eric R. Anschuetz, Sheng-Tao Wang, J. Ignacio Cirac, and Mikhail D. Lukin. Enhancing generative models via quantum correlations, 2021.

[36] Surbhi Goel, Aravind Gollakota, Zhihan Jin, Sushrut Karmalkar, and Adam Klivans. Superpolynomial lower bounds for learning one-layer neural networks using gradient descent. In *International Conference on Machine Learning*, pages 3587–3596. PMLR, 2020.

[37] Aravind Gollakota and Daniel Liang. On the hardness of pac-learning stabilizer states with noise. *Quantum*, 6:640, 2022.

[38] Harper R Grimsley, Sophia E Economou, Edwin Barnes, and Nicholas J Mayhall. An adaptive variational algorithm for exact molecular simulations on a quantum computer. *Nature communications*, 10(1):1–9, 2019.

[39] Jonas Haferkamp. Random quantum circuits are approximate unitary t -designs in depth $o(n t^{5+o(1)})$, 2022.

[40] Aram Harrow and Saeed Mehraban. Approximate unitary t -designs by short random quantum circuits using nearest-neighbor and long-range gates, 2018.

[41] Marcel Hinsche, Marios Ioannou, Alexander Niedner, Jonas Haferkamp, Yihui Quek, Dominik Hangleiter, Jean-Pierre Seifert, Jens Eisert, and Ryan Sweke. Learnability of the output distributions of local quantum circuits. *arXiv preprint arXiv:2110.05517*, 2021.

[42] Hsin-Yuan Huang, Michael Broughton, Masoud Mohseni, Ryan Babbush, Sergio Boixo, Hartmut Neven, and Jarrod R. McClean. Power of data in quantum machine learning. *Nature Communications*, 12(1):2631, May 2021.

[43] Hsin-Yuan Huang, Richard Kueng, and John Preskill. Information-theoretic bounds on quantum advantage in machine learning. *Physical Review Letters*, 126(19):190505, 2021.

[44] Tiefeng Jiang. Maxima of entries of haar distributed matrices. *Probab. Theory Relat. Fields*, 131(1):121–144, 2005.

[45] Michael Kearns. Efficient noise-tolerant learning from statistical queries. *Journal of the ACM (JACM)*, 45(6):983–1006, 1998.

[46] Sumeet Khatri, Ryan LaRose, Alexander Poremba, Lukasz Cincio, Andrew T Sornborger, and Patrick J Coles. Quantum-assisted quantum compiling. *Quantum*, 3:140, 2019.

[47] Bobak Toussi Kiani, Giacomo De Palma, Milad Marvian, Zi-Wen Liu, and Seth Lloyd. Quantum earth mover’s distance: A new approach to learning quantum data, 2021.

[48] Bobak Toussi Kiani, Seth Lloyd, and Reevu Maity. Learning unitaries by gradient descent. *arXiv preprint arXiv:2001.11897*, 2020.

[49] Mária Kieferová and Nathan Wiebe. Tomography and generative training with quantum boltzmann machines. *Phys. Rev. A*, 96:062327, 12 2017.

[50] Joonho Kim, Jaedeok Kim, and Dario Rosa. Universal effectiveness of high-depth circuits in variational eigenproblems, 2020.

[51] Joonho Kim and Yaron Oz. Quantum energy landscape and VQA optimization, 2021.

[52] Diederik P Kingma and Jimmy Ba. Adam: A method for stochastic optimization. *arXiv preprint arXiv:1412.6980*, 2014.

[53] Martin Larocca, Nathan Ju, Diego García-Martín, Patrick J Coles, and M Cerezo. Theory of overparametrization in quantum neural networks. *arXiv preprint arXiv:2109.11676*, 2021.

[54] Yann LeCun, Yoshua Bengio, and Geoffrey Hinton. Deep learning. *nature*, 521(7553):436–444, 2015.

[55] Hao Li, Zheng Xu, Gavin Taylor, Christoph Studer, and Tom Goldstein. Visualizing the loss landscape of neural nets. *Advances in neural information processing systems*, 31, 2018.

[56] Yuanzhi Li and Yingyu Liang. Learning overparameterized neural networks via stochastic gradient descent on structured data. *Advances in Neural Information Processing Systems*, 31, 2018.

[57] Hartmut Maennel, Ibrahim M Alabdulmohsin, Ilya O Tolstikhin, Robert Baldock, Olivier Bousquet, Sylvain Gelly, and Daniel Keysers. What do neural networks learn when trained with random labels? *Advances in Neural Information Processing Systems*, 33:19693–19704, 2020.

[58] Andrea Mari, Thomas R. Bromley, and Nathan Killoran. Estimating the gradient and higher-order derivatives on quantum hardware. *Phys. Rev. A*, 103:012405, 1 2021.

[59] Carlos Ortiz Marrero, Mária Kieferová, and Nathan Wiebe. Entanglement induced barren plateaus, 2020.

[60] Jarrod R. McClean, Sergio Boixo, Vadim N. Smelyanskiy, Ryan Babbush, and Hartmut Neven. Barren plateaus in quantum neural network training landscapes. *Nat. Commun.*, 9(1):4812, 2018.

[61] Kosuke Mitarai, Makoto Negoro, Masahiro Kitagawa, and Keisuke Fujii. Quantum circuit learning. *Physical Review A*, 98(3):032309, 2018.

[62] Kouhei Nakaji and Naoki Yamamoto. Expressibility of the alternating layered ansatz for quantum computation. *Quantum*, 5:434, 2021.

[63] John Napp. Quantifying the barren plateau phenomenon for a model of unstructured variational ansätze, 2022.

[64] Behnam Neyshabur, Srinadh Bhojanapalli, David McAllester, and Nati Srebro. Exploring generalization in deep learning. *Advances in neural information processing systems*, 30, 2017.

[65] Adam Paszke, Sam Gross, Francisco Massa, Adam Lerer, James Bradbury, Gregory Chanan, Trevor Killeen, Zeming Lin, Natalia Gimelshein, Luca Antiga, Alban Desmaison, Andreas Kopf, Edward Yang, Zachary DeVito, Martin Raison, Alykhan Tejani, Sasank Chilamkurthy, Benoit Steiner, Lu Fang, Junjie Bai, and Soumith Chintala. Pytorch: An imperative style, high-performance deep learning library. In H. Wallach, H. Larochelle, A. Beygelzimer, F. d’Alché-Buc, E. Fox, and R. Garnett, editors, *Advances in Neural Information Processing Systems 32*, pages 8024–8035. Curran Associates, Inc., 2019.

[66] Alberto Peruzzo, Jarrod McClean, Peter Shadbolt, Man-Hong Yung, Xiao-Qi Zhou, Peter J Love, Alán Aspuru-Guzik, and Jeremy L O’brien. A variational eigenvalue solver on a photonic quantum processor. *Nature communications*, 5(1):1–7, 2014.

[67] Arthur Pesah, M Cerezo, Samson Wang, Tyler Volkoff, Andrew T Sornborger, and Patrick J Coles. Absence of barren plateaus in quantum convolutional neural networks. *Physical Review X*, 11(4):041011, 2021.

[68] John Preskill. Quantum Computing in the NISQ era and beyond. *Quantum*, 2:79, 8 2018.

[69] Lev Reyzin. Statistical queries and statistical algorithms: Foundations and applications. *arXiv preprint arXiv:2004.00557*, 2020.

[70] Maria Schuld, Ville Bergholm, Christian Gogolin, Josh Izaac, and Nathan Killoran. Evaluating analytic gradients on quantum hardware. *Physical Review A*, 99(3):032331, 2019.

[71] Huitao Shen, Pengfei Zhang, Yi-Zhuang You, and Hui Zhai. Information scrambling in quantum neural networks. *Physical Review Letters*, 124(20):200504, 2020.

[72] Sukin Sim, Peter D Johnson, and Alán Aspuru-Guzik. Expressibility and entangling capability of parameterized quantum circuits for hybrid quantum-classical algorithms. *Advanced Quantum Technologies*, 2(12):1900070, 2019.

[73] Andrea Skolik, Jarrod R McClean, Masoud Mohseni, Patrick van der Smagt, and Martin Leib. Layerwise learning for quantum neural networks. *Quantum Machine Intelligence*, 3(1):1–11, 2021.

[74] James Stokes, Josh Izaac, Nathan Killoran, and Giuseppe Carleo. Quantum natural gradient. *Quantum*, 4:269, 2020.

[75] Balázs Szörényi. Characterizing statistical query learning: simplified notions and proofs. In *International Conference on Algorithmic Learning Theory*, pages 186–200. Springer, 2009.

[76] Leslie G Valiant. A theory of the learnable. *Communications of the ACM*, 27(11):1134–1142, 1984.

[77] Dan Voiculescu. Limit laws for random matrices and free products. *Invent. Math.*, 104(1):201–220, 1991.

[78] Xin Wang, Zhixin Song, and Youle Wang. Variational quantum singular value decomposition. *Quantum*, 5:483, 2021.

[79] Roeland Wiersema, Cunlu Zhou, Yvette de Sereville, Juan Felipe Carrasquilla, Yong Baek Kim, and Henry Yuen. Exploring entanglement and optimization within the hamiltonian variational ansatz. *PRX Quantum*, 1(2):020319, 2020.

[80] David H Wolpert and William G Macready. No free lunch theorems for optimization. *IEEE transactions on evolutionary computation*, 1(1):67–82, 1997.

[81] Xuchen You and Xiaodi Wu. Exponentially many local minima in quantum neural networks. In *International Conference on Machine Learning*, pages 12144–12155. PMLR, 2021.

[82] A. Yu. Zaitsev. Estimates for the Levy-Prokhorov distance in terms of characteristic functions and some of their applications. *J. Sov. Math.*, 27(5):3070–3083, 1984.

[83] Chiyuan Zhang, Samy Bengio, Moritz Hardt, Benjamin Recht, and Oriol Vinyals. Understanding deep learning (still) requires rethinking generalization. *Communications of the ACM*, 64(3):107–115, 2021.

[84] Christa Zoufal, Aurélien Lucchi, and Stefan Woerner. Variational quantum Boltzmann machines. *Quantum Mach. Intell.*, 3(1):7–21, 2021.

A Training Error Dominates in the Optimization of Variational Quantum Algorithms

VQE is purely a problem of optimization and may appear unrelated to the challenges in learning via variational algorithms; however, by decomposing the error of a learning algorithm into key terms using well-established methods [14], we will show that variational learning algorithms essentially face the same optimization task and its associated challenges. In both cases, the hardness of learning or optimizing with variational circuits manifests itself in the challenges of optimizing over a cost landscape riddled with traps (or other barriers to optimization).

We restrict ourselves here to the supervised learning framework of empirical risk minimization, where our goal is to learn a space of input and output pairs $(\mathbf{x}, \mathbf{y}) \in \mathcal{X} \times \mathcal{Y}$ drawn from a distribution $P(\mathbf{x}, \mathbf{y})$. Given a loss function $\ell : \mathcal{Y} \times \mathcal{Y} \rightarrow [0, \infty)$, we quantify how well our function performs by considering the expected risk \mathcal{R} :

$$\mathcal{R}(f) = \mathbb{E}_{\mathbf{x}} [\ell(f(\mathbf{x}), f^*(\mathbf{x}))], \quad (\text{A.1})$$

where the expectation above is taken with respect to $P(\mathbf{x}, \mathbf{y})$. To benchmark performance, we compare to the “optimal” or target function f^* which is the minimizer of the risk:

$$f^*(\mathbf{x}) = \arg \min_{\hat{\mathbf{y}} \in \mathcal{Y}} \mathbb{E} [\ell(\mathbf{y}, \hat{\mathbf{y}}) | \mathbf{x}]. \quad (\text{A.2})$$

To perform learning, we search for a function $\hat{f} \in \mathcal{F}$ in the function class \mathcal{F} (think *e.g.*, the set of functions expressed by quantum neural networks). The expected risk $\mathcal{R}(f)$ is not something one can calculate since it requires access to the full probability distribution of the data. Instead, one minimizes the empirical risk $\widehat{\mathcal{R}}(f)$ (often named the training error) over a given training data set \mathcal{D} of size N consisting of pairs $\{\mathbf{x}_i, \mathbf{y}_i\}_{i=1}^N$:

$$\widehat{\mathcal{R}}(f) = \sum_{i=1}^N \ell(f(\mathbf{x}_i), f^*(\mathbf{x}_i)). \quad (\text{A.3})$$

Note that we use the hat in $\widehat{\mathcal{R}}$ and \widehat{f} to denote the expected risk measure and function that one actually has access to during training or optimization. Given the above, one can bound the expected risk of any function \widehat{f} as a decomposition below [14]:

$$\mathbb{E} [\mathcal{R}(\widehat{f}) - \mathcal{R}(f^*)] \leq \underbrace{\min_{f \in \mathcal{F}} \mathcal{R}(f) - \mathcal{R}(f^*)}_{\text{approximation error}} + \underbrace{2\mathbb{E} \left[\sup_{f \in \mathcal{F}} |\mathcal{R}(f) - \widehat{\mathcal{R}}(f)| \right]}_{\text{generalization error}} + \underbrace{\mathbb{E} [\widehat{\mathcal{R}}(\widehat{f}) - \min_{f \in \mathcal{F}} \widehat{\mathcal{R}}(f)]}_{\text{optimization error}}, \quad (\text{A.4})$$

where the expectation above is taken with respect to the distribution over data sets or training sets. The proof of this statement follows by a careful, yet straightforward, application of additions/subtractions with corresponding bounds [14].

Proof. Let $\widehat{f}_{\mathcal{F}} = \arg \min_{f \in \mathcal{F}} \widehat{\mathcal{R}}(f)$ and $f_{\mathcal{F}} = \arg \min_{f \in \mathcal{F}} \mathcal{R}(f)$. Then, by adding and subtracting quantities, we obtain the following result:

$$\begin{aligned} \mathbb{E} [\mathcal{R}(\widehat{f}) - \mathcal{R}(f^*)] &= \mathbb{E} [\mathcal{R}(\widehat{f}) - \mathcal{R}(f^*) \\ &\quad + \widehat{\mathcal{R}}(\widehat{f}_{\mathcal{F}}) - \widehat{\mathcal{R}}(\widehat{f}_{\mathcal{F}}) \\ &\quad + \mathcal{R}(f_{\mathcal{F}}) - \mathcal{R}(f_{\mathcal{F}}) + \widehat{\mathcal{R}}(f_{\mathcal{F}}) - \widehat{\mathcal{R}}(f_{\mathcal{F}}) \\ &\quad + \widehat{\mathcal{R}}(\widehat{f}) - \widehat{\mathcal{R}}(\widehat{f})]. \end{aligned} \quad (\text{A.5})$$

We reorder the above as follows and note their relation to the main statement:

$$\mathbb{E} [\mathcal{R}(\hat{f}) - \mathcal{R}(f^*)] = \mathbb{E} [\mathcal{R}(f_{\mathcal{F}}) - \mathcal{R}(f^*)] \quad \text{approximation error} \quad (\text{A.6})$$

$$+ \mathbb{E} [\mathcal{R}(\hat{f}) - \hat{\mathcal{R}}(\hat{f})] \quad \text{generalization error} \quad (\text{A.7})$$

$$+ \mathbb{E} [\hat{\mathcal{R}}(f_{\mathcal{F}}) - \mathcal{R}(f_{\mathcal{F}})] \quad \text{generalization error} \quad (\text{A.8})$$

$$+ \mathbb{E} [\hat{\mathcal{R}}(\hat{f}_{\mathcal{F}}) - \hat{\mathcal{R}}(f_{\mathcal{F}})] \leq 0 \text{ since } \hat{f}_{\mathcal{F}} \text{ minimizes } \hat{\mathcal{R}} \quad (\text{A.9})$$

$$+ \mathbb{E} [\hat{\mathcal{R}}(\hat{f}) - \hat{\mathcal{R}}(\hat{f}_{\mathcal{F}})] \quad \text{optimization error} \quad (\text{A.10})$$

For the quantities in the generalization error, we have since $\hat{f}, f_{\mathcal{F}} \in \mathcal{F}$:

$$\begin{aligned} \mathbb{E} [\mathcal{R}(\hat{f}) - \hat{\mathcal{R}}(\hat{f})] &\leq \mathbb{E} \left[\sup_{f \in \mathcal{F}} |\mathcal{R}(f) - \hat{\mathcal{R}}(f)| \right] \\ \mathbb{E} [\hat{\mathcal{R}}(f_{\mathcal{F}}) - \mathcal{R}(f_{\mathcal{F}})] &\leq \mathbb{E} \left[\sup_{f \in \mathcal{F}} |\mathcal{R}(f) - \hat{\mathcal{R}}(f)| \right]. \end{aligned} \quad (\text{A.11})$$

Plugging these into equation A.5 and noting as before that $\mathbb{E} [\hat{\mathcal{R}}(\hat{f}_{\mathcal{F}}) - \hat{\mathcal{R}}(f_{\mathcal{F}})] \leq 0$, we arrive at the desired result. \square

In the context of quantum variational algorithms, each of these has the following properties:

- The **approximation error** quantifies how well the most optimal function in the hypothesis class \mathcal{F} can fit the function. In variational settings, the approximation error is typically bounded by assuming the target function is generated from a nice class of functions (e.g. shallow circuits) or arguing either analytically or theoretically that a given ansatz can (approximately) express the target function [62, 72, 31, 71].
- The **generalization error** quantifies the statistical error that arises from having a finite data set and is typically insignificant in quantum variational algorithms where circuit complexity is limited with regards to the number of training samples. More precisely, for data sets of size m , previous work [18, 32] bound the generalization error as $\tilde{O}(\sqrt{|G|/m})$ where $|G|$ is the number of trainable gates. In contrast, generalization error in heavily overparameterized classical neural network models are challenging to bound and it is still an open question why deep learning models generalize so well [83, 64].
- The **optimization error** measures how well one is able to reduce the empirical risk. Issues with optimization such as poor local minima and barren plateaus arise here. Note that there is a distinct difference between quantum and classical deep learning here. With classical deep neural networks, this quantity is typically negligible since neural networks are overparameterized with respect to the data set size and can fit random data arbitrarily well [83, 57]. Furthermore, due to efficient means of calculating gradients with bit-level precision, classical machine learning algorithms perform optimization over parameters far more efficiently than quantum variational algorithms. In quantum variational models, overparameterization with respect to the Hilbert space dimension is generally needed to arbitrarily fit data [5, 79, 48]. Since the Hilbert space dimension grows exponentially with the number of qubits, such overparameterization becomes prohibitive rather rapidly.

In summary, the approximation error and generalization error can be bounded efficiently with sufficient data so failures in learning are typically related to optimization over the empirical risk. As an aside, this is loosely analogous to the classical setting of learning polynomial size Boolean circuits which is strongly conjectured to be hard since the space of Boolean functions is challenging to search over [7].

Finally, we would like to stress that the decomposition of the excess risk performed in this section is neither unique nor necessarily tight. The decomposition can be performed in various other ways depending on the quantities one would like to bound. We chose the decomposition here to relate errors in quantum machine learning algorithms to their classical counterparts and to highlight the challenges one may face when attempting to *provably* learn a target function class.

B Review and Brief History of the Statistical Query Framework

The statistical query (SQ) framework was introduced nearly 25 years ago to analyze the hardness of learning problems [45]. This framework restricts algorithms to a series of noisy queries, and hardness results are stated in terms of the number of queries needed to learn a given class of functions. Since there are various different ways of defining the statistical query model—including a recent quantum oracular version proposed in [10]—let us first review some of the various models considered in prior work.

1. **Classical statistical query model:** Introduced by [45], this was the first statistical query model introduced. For a given distribution D of inputs over an input space X and target concept $c : X \rightarrow \{-1, +1\}$, one can make a statistical query $\text{SQ}(q, \tau)$, by providing a threshold $\tau \in \mathbb{R}^+$ and a query function $q : X \times \{-1, +1\} \rightarrow \{-1, +1\}$. The query returns a value in the range:

$$\mathbb{E}_{x \sim D} [q(x, c(x)) - \tau] \leq \text{SQ}(q, \tau) \leq \mathbb{E}_{x \sim D} [q(x, c(x)) + \tau]. \quad (\text{B.1})$$

2. **Correlational statistical query model:** The query is the same as before, except now, one queries correlations $\text{CSQ}(q, \tau)$ only by providing a threshold $\tau \in \mathbb{R}^+$ and a query function $h : X \rightarrow \{-1, +1\}$. The query returns a value in the range:

$$\mathbb{E}_{x \sim D} [h(x)c(x) - \tau] \leq \text{CSQ}(h, \tau) \leq \mathbb{E}_{x \sim D} [h(x)c(x) + \tau]. \quad (\text{B.2})$$

This model is strictly less powerful than the standard statistical query model since one can perform a correlational statistical query with a standard statistical query [75].

3. **Quantum statistical query model:** This is a statistical query model with quantum samples [10]. Here, we are restricted to target (classical) Boolean functions $c : \{0, 1\}^n \rightarrow \{-1, +1\}$. A quantum statistical query $\text{Qstat}(\tau, M)$ is provided with a threshold $\tau \in \mathbb{R}^+$ and an observable or Hamiltonian $M \in (\mathbb{C}^2)^{n+1} \times (\mathbb{C}^2)^{n+1}$ satisfying $\|M\| \leq 1$ and returns a number in the range:

$$\langle \psi_c | M | \psi_c \rangle - \tau \leq \text{Qstat}(M, \tau) \leq \langle \psi_c | M | \psi_c \rangle + \tau, \quad (\text{B.3})$$

where $|\psi_c\rangle = \sum_{x \in \{0, 1\}^n} \sqrt{D(x)} |x\rangle |c(x)\rangle$. This model is useful to analyze the hardness of learning classical Boolean functions when given the extra power of querying the classical function in superposition. Our work considers learning quantum data and thus does not fit into the framework of this SQ model.

The SQ learning setting is related to the probably approximately correct (PAC) setting of learning theory [76] in that if an algorithm can learn a given function class in the SQ learning setting under any input distribution, then that function class is also PAC learnable [45, 69]. Two very recent works have studied the SQ hardness of learning data generated by quantum circuits. First, [41] analyze the hardness of learning the output distribution of clifford circuits and stabilizer states showing that these distributions are hard to learn using classical Boolean SQ oracles. Nevertheless, when given samples from the Boolean hypercube of the distribution, they provide an efficient algorithm based on linear regression to determine the stabilizer state underlying the distribution. Such a result is similar to classic results in [45] showing that parity functions are hard to learn using only SQ oracle calls but easy when performing linear regression with enough samples. Second, [37] show that learning stabilizer states is hard in an SQ setting where queries are made over two-outcome POVMs. Their results show that learning stabilizer states in such a setting is as hard as learning the function class of parity with noise in the standard Boolean setting. Our results expand the set of quantum functions that are hard to learn in SQ settings and relate such hardness results to the variational setting.

B.1 Limitations of Hardness Results in the SQ Framework

Though the SQ framework is a useful tool for analyzing the hardness of learning a class of functions in noisy settings, there are a few caveats and limitations of any hardness results proven in the SQ setting:

- The statistical query model inherently requires noise in the form of the tolerance τ . Furthermore, the guarantees of learning must handle worst case noise scenarios where the noise acts adversarially on the statistical query. Though quantum variational algorithms are inherently noisy, this noise typically does not arise in an adversarial nature.
- The statistical query model places bounds on learning classes of functions using optimizers that query this SQ model and is not directly related to issues of loss landscapes since there is no loss landscape to actually optimize. Nevertheless, since (noisy) calculations of gradients and loss function values are themselves examples of statistical queries, any issues with optimizing over a loss landscape will also arise in performing the optimizer through a series of statistical queries.
- Learning every function in a class \mathcal{C} can be restrictive, and in practice, one may only really want to learn a given function or a small set of functions. In fact, it can be shown that even the class of functions generated by shallow neural networks is hard to learn in the SQ setting [30, 36]; nevertheless, neural networks are very successful at learning specific functions such as the classification of real-world images [54].

C Proofs of Statistical Query Results

Throughout this section, we make use of standard formulas from Weingarten calculus to integrate over Haar measure or t -designs [63, 26, 27]. Let $|I_m^n\rangle$ denote n copies of the unnormalized maximally mixed state on a Hilbert space of dimension m :

$$|I_m^n\rangle = \sum_{i_1, i_2, \dots, i_n=1}^m |i_1, i_2, \dots, i_n\rangle |i_1, i_2, \dots, i_n\rangle. \quad (\text{C.1})$$

For $n = 2$, let $|S_m^2\rangle$ denote the same unnormalized state as above with a swap operation applied to the second register:

$$\begin{aligned} |S_m^2\rangle &= (\mathbf{I} \otimes \text{SWAP}) |I_m^2\rangle \\ &= \sum_{i_1, i_2=1}^m |i_1, i_2\rangle |i_2, i_1\rangle. \end{aligned} \quad (\text{C.2})$$

The following hold over a distribution \mathcal{D} that is a 2-design over the unitary matrices of dimension m :

$$\begin{aligned} \mathbb{E}_{\mathbf{U} \sim \mathcal{D}} [\mathbf{U} \otimes \bar{\mathbf{U}}] &= \frac{1}{m} |I_m^1\rangle \langle I_m^1|, \\ \mathbb{E}_{\mathbf{U} \sim \mathcal{D}} [\mathbf{U} \otimes \mathbf{U} \otimes \bar{\mathbf{U}} \otimes \bar{\mathbf{U}}] &= \frac{1}{m^2 - 1} (|I_m^2\rangle \langle I_m^2| + |S_m^2\rangle \langle S_m^2|) - \frac{1}{m(m^2 - 1)} (|I_m^2\rangle \langle S_m^2| + |S_m^2\rangle \langle I_m^2|), \end{aligned} \quad (\text{C.3})$$

where $\bar{\mathbf{U}}$ denotes the matrix with entries that are the complex conjugate of entries of \mathbf{U} .

As a simple example of applying the techniques above, we show that for unitaries \mathbf{U}_* and \mathbf{V} of dimension d^n (e.g., $d = 2$ for qubits and n is the number of qubits), $\mathbb{E}_{\rho \sim \mathcal{D}} [\text{Re}[\text{Tr}(\mathbf{U}_*^\dagger \mathbf{V} \rho)]] = d^{-n} \text{Re}[\text{Tr}(\mathbf{U}_*^\dagger \mathbf{V})]$ whenever \mathcal{D} forms a 1-design. This is a crucial formula that we use in the evaluation of statistical queries to qUSQ.

Lemma C.1. *For any distribution \mathcal{D} that is a 1-design over states of dimension d^n ,*

$$\mathbb{E}_{\rho \sim \mathcal{D}} [\text{Re}[\text{Tr}(\mathbf{W}^\dagger \mathbf{V} \rho)]] = d^{-n} \text{Re}[\text{Tr}(\mathbf{W}^\dagger \mathbf{V})]. \quad (\text{C.4})$$

Proof. WLOG, we rewrite the equation above in terms of a distribution over pure states and with a slight abuse of notation, we let \mathcal{D} also denote a distribution over unitary matrices \mathbf{U} that forms a 1-design:

$$\mathbb{E}_{\rho \sim \mathcal{D}} [\text{Re}[\text{Tr}(\mathbf{W}^\dagger \mathbf{V} \rho)]] = \mathbb{E}_{\mathbf{U} \sim \mathcal{D}} [\text{Re}[\langle 0 | \mathbf{U}^\dagger \mathbf{W}^\dagger \mathbf{V} \mathbf{U} | 0 \rangle]]. \quad (\text{C.5})$$

Using equation C.1, we have:

$$\mathbb{E}_{\mathbf{U} \sim \mathcal{D}} [\text{Re}[\langle 0 | \mathbf{U}^\dagger \mathbf{W}^\dagger \mathbf{V} \mathbf{U} | 0 \rangle]] = \mathbb{E}_{\mathbf{U} \sim \mathcal{D}} [\langle I_{d^n}^1 | ((\mathbf{W}^\dagger \mathbf{V}) \otimes \mathbf{I}) (\mathbf{U} \otimes \bar{\mathbf{U}}) | 0 \rangle | 0 \rangle]. \quad (\text{C.6})$$

Applying equation C.3, we have:

$$\begin{aligned} \mathbb{E}_{\mathbf{U} \sim \mathcal{D}} [\text{Re}[\langle 0 | \mathbf{U}^\dagger \mathbf{W}^\dagger \mathbf{V} \mathbf{U} | 0 \rangle]] &= \mathbb{E}_{\mathbf{U} \sim \mathcal{D}} [\text{Re}[\langle I_{d^n}^1 | ((\mathbf{W}^\dagger \mathbf{V}) \otimes \mathbf{I}) (\mathbf{U} \otimes \bar{\mathbf{U}}) | 0 \rangle | 0 \rangle]] \\ &= \frac{1}{d^n} \text{Re}[\langle I_{d^n}^1 | ((\mathbf{W}^\dagger \mathbf{V}) \otimes \mathbf{I}) | I_{d^n}^1 \rangle \langle I_{d^n}^1 | 0 \rangle | 0 \rangle] \\ &= \frac{1}{d^n} \text{Re}[\text{Tr}(\mathbf{W}^\dagger \mathbf{V})]. \end{aligned} \quad (\text{C.7})$$

□

C.1 Lower Bounds for Statistical Query Learning

For completeness, we include a proof of Theorem 3.3, copied below, which lower bounds the number of queries needed to learn a hypothesis class. qCSQ and qUSQ both take the form of an inner product so the proof holds for both cases. As a reminder we include the definitions of qCSQ and qUSQ below.

Quantum correlational statistical query (qCSQ) Given a target observable \mathbf{M} and a distribution \mathcal{D} of input states, a query qCSQ(\mathbf{O}, τ) takes in a bounded observable \mathbf{O} with $\|\mathbf{O}\| \leq 1$ and a tolerance τ and returns a value in the range:

$$\mathbb{E}_{\rho \sim \mathcal{D}} [\text{Tr}(\mathbf{O} \rho) \text{Tr}(\mathbf{M} \rho) - \tau] \leq \text{qCSQ}(\mathbf{O}, \tau) \leq \mathbb{E}_{\rho \sim \mathcal{D}} [\text{Tr}(\mathbf{O} \rho) \text{Tr}(\mathbf{M} \rho) + \tau]. \quad (\text{C.8})$$

Quantum unitary statistical query (qUSQ) Given a target unitary transformation \mathbf{U}_* over a distribution \mathcal{D} of inputs, the oracle qUSQ(\mathbf{V}, τ) takes in a unitary matrix \mathbf{V} and a tolerance τ and returns a value in the range:

$$\mathbb{E}_{\rho \sim \mathcal{D}} [\text{Re}[\text{Tr}(\mathbf{U}_*^\dagger \mathbf{V} \rho)] - \tau] \leq \text{qUSQ}(\mathbf{V}, \tau) \leq \mathbb{E}_{\rho \sim \mathcal{D}} [\text{Re}[\text{Tr}(\mathbf{U}_*^\dagger \mathbf{V} \rho)] + \tau]. \quad (\text{C.9})$$

Finally, we remind the reader of the definition of the statistical query dimension.

Definition 3.2 (Statistical query dimension [13, 69]). For a distribution \mathcal{D} and concept class \mathcal{H} where $\|\mathbf{M}\|_{\mathcal{D}}^2 \leq C_{\max}$ for all $\mathbf{M} \in \mathcal{H}$, the statistical query dimension (SQ-DIM $_{\mathcal{D}}(\mathcal{H})$) is the largest positive integer d such that there exists d observables $\mathbf{M}_1, \mathbf{M}_2, \dots, \mathbf{M}_d \in \mathcal{H}$ such that for all $i \neq j : |\langle \mathbf{M}_i, \mathbf{M}_j \rangle_{\mathcal{D}}| \leq C_{\max}/d$.

From here, we provide a proof of the query complexity of learning a function class, similar to the proof in [75].

Theorem 3.3 (Query complexity of learning [75, 13]). *Given a distribution \mathcal{D} on inputs and a hypothesis class \mathcal{H} where $\|\mathbf{M}\|_{\mathcal{D}}^2 \leq C_{\max}$ for all $\mathbf{M} \in \mathcal{H}$, let $d = \text{SQ-DIM}_{\mathcal{D}}(\mathcal{H})$ be the statistical query dimension of \mathcal{H} . Any qCSQ or qUSQ learner making queries with tolerance $C_{\max}\tau$ must make at least $(d\tau^2 - 1)/2$ queries to learn \mathcal{H} up to error $C_{\max}\tau$.*

Proof. Since we are restricted to the weaker setting of correlational statistical queries in this study, we can reuse a simple and elegant proof from [75].

Let $\mathbf{M}_1, \mathbf{M}_2, \dots, \mathbf{M}_d$ be d functions that saturate $\text{SQ-DIM}_{\mathcal{D}}(\mathcal{H})$, i.e., $\langle \mathbf{M}_i, \mathbf{M}_j \rangle_{\mathcal{D}} \leq 1/d$ for all $i \neq j$. Assume we apply query \mathbf{O} and let $S = \{i \in [d] : \langle \mathbf{O}, \mathbf{M}_i \rangle_{\mathcal{D}} > C_{\max} \tau\}$. Then, by simple application of Cauchy-Schwarz, we have that for any query \mathbf{O} :

$$\begin{aligned} \left\langle \mathbf{O}, \sum_{i \in S} \mathbf{M}_i \right\rangle_{\mathcal{D}}^2 &\leq C_{\max} \left\| \sum_{i \in S} \mathbf{M}_i \right\|_{\mathcal{D}}^2 \\ &= C_{\max} \sum_{i, j \in S} \langle \mathbf{M}_i, \mathbf{M}_j \rangle_{\mathcal{D}} \\ &\leq C_{\max}^2 (|S| + |S|^2/d). \end{aligned} \tag{C.10}$$

Note, that we can also bound the quantity above from below by using the definition of S :

$$\left\langle \mathbf{O}, \sum_{i \in S} \mathbf{M}_i \right\rangle_{\mathcal{D}} \geq C_{\max} |S| \tau. \tag{C.11}$$

Combining the above, we have that

$$|S| \leq d/(dC_{\max}^2 \tau^2 - 1). \tag{C.12}$$

Similarly, defining $S' = \{i \in [d] : \langle \mathbf{O}, \mathbf{M}_i \rangle_{\mathcal{D}} < -C_{\max} \tau\}$ with correlation less than $-\tau$, we follow the steps above to also note that $|S'| \leq d/(dC_{\max}^2 \tau^2 - 1)$. Altogether, we have that $|S'| + |S| \leq 2d/(dC_{\max}^2 \tau^2 - 1)$, which implies that each oracle call can only eliminate up to $2d/(dC_{\max}^2 \tau^2 - 1)$ functions. Since we must eliminate at least d functions to learn the target class, we arrive at the desired bound. \square

C.2 Proofs of Statistical Query Dimensions for Variational Function Classes

Proposition C.2 (SQ dimension for $L = 1$ and fixed global measurement). *Given n qubits, let \mathcal{H} be the concept class containing functions $f : \mathbb{C}^{2^n} \rightarrow \mathbb{R}$ consisting of single qubit rotations followed by a global Pauli Z measurement, i.e. functions of the form*

$$f(|\psi\rangle; \mathbf{U}_1, \mathbf{U}_2, \dots, \mathbf{U}_n) = \langle \psi | (\mathbf{U}_1^\dagger \otimes \mathbf{U}_2^\dagger \otimes \dots \otimes \mathbf{U}_n^\dagger) (\mathbf{Z}_1 \otimes \mathbf{Z}_2 \otimes \dots \otimes \mathbf{Z}_n) (\mathbf{U}_1 \otimes \mathbf{U}_2 \otimes \dots \otimes \mathbf{U}_n) |\psi\rangle, \tag{C.13}$$

where $|\psi\rangle$ is the input to the function and $\mathbf{U}_1, \mathbf{U}_2, \dots, \mathbf{U}_n$ are the parameterized 1-qubit rotation operations on distinct qubits. Then, the concept class \mathcal{H} has SQ dimension $\text{SQ-DIM}_{\mathcal{D}}(\mathcal{H}) \geq 3^n$ under any distribution of states that forms a 2-design.

Proof. The simple proof of this proposition relies on the fact that all Pauli operators are pairwise orthogonal for a 2-design, i.e. given two distinct Pauli operators \mathbf{P}_1 and \mathbf{P}_2 then $\mathbb{E}_{\rho \sim \mathcal{D}} [\text{Tr}(\mathbf{P}_1 \rho) \text{Tr}(\mathbf{P}_2 \rho)] = 0$. Therefore, we simply show that the concept class \mathcal{H} is capable of producing any Pauli string not containing the identity.

To proceed, note that we can rewrite the function class as follows:

$$f(|\psi\rangle; \mathbf{U}_1, \mathbf{U}_2, \dots, \mathbf{U}_n) = \langle \psi | (\mathbf{U}_1^\dagger \mathbf{Z}_1 \mathbf{U}_1) \otimes (\mathbf{U}_2^\dagger \mathbf{Z}_2 \mathbf{U}_2) \otimes \dots \otimes (\mathbf{U}_n^\dagger \mathbf{Z}_n \mathbf{U}_n) |\psi\rangle. \tag{C.14}$$

To obtain any arbitrary Pauli string, we simply conjugate the \mathbf{Z}_i operator for the i -th qubit by a corresponding operation. If the i -th qubit of a Pauli string is equal to \mathbf{X} , then we set $\mathbf{U}_i = \mathbf{H}$ or the Hadamard transform. Similarly, if the i -th qubit of a Pauli string is equal to \mathbf{Y} , then we set $\mathbf{U}_i = \mathbf{H} \sqrt{\mathbf{Z}}^\dagger$. By conjugation of the individual 1-qubit operators, we thus can produce any Pauli operator in $\{\mathbf{X}, \mathbf{Y}, \mathbf{Z}\}^{\otimes n}$. \square

Corollary C.3. *By application of Theorem 3.3, the class of functions defined in Proposition C.2 consisting of a single layer of parameterized single qubit unitary gates and a fixed global measurement on n qubits requires $2^{\Omega(n)}$ queries to learn for a query tolerance greater than $3^{-\beta n}$, where $\beta = 1/2 - \Omega(1)$.*

Proposition C.4 (SQ dimension for $L = \lceil \log_2 n \rceil$, two-qubit gates, and single Pauli \mathbf{Z} measurement). *Given n qubits, let \mathcal{H} be the concept class containing functions $f : \mathbb{C}^{2^n} \rightarrow \mathbb{R}$ consisting of $\lceil \log_2 n \rceil$ layers of two-qubit gates followed by a Pauli \mathbf{Z} measurement on a single qubit. Then, the concept class \mathcal{H} has SQ dimension $\text{SQ-DIM}_{\mathcal{D}}(\mathcal{H}) \geq 4^n - 1$ under any distribution of inputs that forms a 2-design.*

Proof. We will show that \mathcal{H} is powerful enough to perform any nontrivial Pauli measurement (i.e., any Pauli but the identity) and hence construct at least $4^n - 1$ orthogonal functions. Classically, any parity function can be constructed in $\lceil \log_2 n \rceil$ layers, and we use a similar construction here.

Without loss of generality, assume the Pauli measurement is on the first qubit. Let $\mathbf{U}(\theta)$ represent a possible unitary that can be applied using the given hypothesis class, resulting in a final measurement of $\mathbf{U}(\theta)^\dagger \mathbf{Z}_1 \mathbf{U}(\theta)$ on a given input state $|\psi\rangle$. We will show that we can parameterize the circuit such that for any Pauli measurement, $\mathbf{P}_1 \otimes \mathbf{P}_2 \otimes \cdots \otimes \mathbf{P}_n = \mathbf{U}(\theta)^\dagger \mathbf{Z}_1 \mathbf{U}(\theta)$ where \mathbf{P}_i indicates the Pauli operator of qubit i (i.e., $\mathbf{P}_i \in \{\mathbf{I}, \mathbf{X}, \mathbf{Y}, \mathbf{Z}\}$).

To construct any Pauli operator $\mathbf{P}_1 \otimes \mathbf{P}_2 \otimes \cdots \otimes \mathbf{P}_n$, we follow the steps below:

1. In the first layer, apply a unitary to each qubit i which maps the computational basis to the basis of the Pauli for qubit i . In more detail, if $\mathbf{P}_i = \mathbf{I}$ or $\mathbf{P}_i = \mathbf{Z}$, then apply the identity map to keep the basis the same. If $\mathbf{P}_i = \mathbf{X}$, then apply the Hadamard transform and if $\mathbf{P}_i = \mathbf{Y}$ then apply the operation $\mathbf{H} \sqrt{\mathbf{Z}}^\dagger$.
2. In the l -th layer, apply a specific two qubit gate to qubit pairs $\{1, 2^{l-1} + 1\}, \{2(2^{l-1}) + 1, 3(2^{l-1}) + 1\}, \{4(2^{l-1}) + 1, 5(2^{l-1}) + 1\}, \dots$. For a layer l and a given pair $\{i, j\}$, apply the following gate:
 - if all of $\mathbf{P}_i, \mathbf{P}_{i+1}, \dots, \mathbf{P}_{j+2^{l-1}}$ are equal to \mathbf{I} , then apply the identity.
 - if any of $\mathbf{P}_i, \mathbf{P}_{i+1}, \dots, \mathbf{P}_{j-1}$ are not equal to \mathbf{I} and all of $\mathbf{P}_j, \mathbf{P}_{j+1}, \dots, \mathbf{P}_{j+2^{l-1}}$ are equal to \mathbf{I} then apply the identity as well.
 - if all of $\mathbf{P}_i, \mathbf{P}_{i+1}, \dots, \mathbf{P}_{j-1}$ are equal to \mathbf{I} and any of $\mathbf{P}_j, \mathbf{P}_{j+1}, \dots, \mathbf{P}_{j+2^{l-1}}$ are not equal to \mathbf{I} , then apply a swap gate between qubits i and j .
 - otherwise, apply the following 2-qubit gate to i and j which conjugates $\mathbf{Z} \otimes \mathbf{I}$ to $\mathbf{Z} \otimes \mathbf{Z}$:

$$\begin{bmatrix} 1 & 0 & 0 & 0 \\ 0 & 0 & 0 & 1 \\ 0 & 0 & 1 & 0 \\ 0 & 1 & 0 & 0 \end{bmatrix}. \quad (\text{C.15})$$

3. repeat step 2 above starting from $l = 1$ to $l = \lceil \log_2 n \rceil$. Measuring the first qubit will measure the corresponding desired Pauli. Note, that the single qubit operations of step 1 and the two-qubit operations of step 2 can be combined into a single 2-qubit gate thus not changing the depth.

Following the steps above, at layer l , the measurement of the first qubit corresponds to the Pauli measurement of the first 2^l qubits. Recursively applying this procedure l layers produces any arbitrary Pauli string. \square

Corollary C.5. *By application of Theorem 3.3, the class of functions defined in Proposition C.4 consisting of $\lceil \log_2 n \rceil$ two-qubit unitary gates and a fixed measurement on a single qubit requires $2^{\Omega(n)}$ queries to learn for a query tolerance greater than $4^{-\beta n}$, where $\beta = 1/2 - \Omega(1)$.*

Proposition C.6 (SQ dimension for L layers, neighboring 2-local gates in one-dimensional lattice and fixed single qubit measurement). *Given n qubits, let \mathcal{H} be the concept class containing functions $f : \mathbb{C}^{2^n} \rightarrow \mathbb{R}$ consisting of L layers of 2-qubit unitary operations followed by a Pauli \mathbf{Z} measurement on a single qubit (labeled qubit m), i.e. functions of the form*

$$f(|\psi\rangle; \mathbf{W}_1, \mathbf{W}_2, \dots, \mathbf{W}_L) = \langle \psi | \mathbf{W}_1^\dagger \mathbf{W}_2^\dagger \cdots \mathbf{W}_L^\dagger (\mathbf{Z}_m) \mathbf{W}_L \cdots \mathbf{W}_2 \mathbf{W}_1 | \psi \rangle, \quad (\text{C.16})$$

where $|\psi\rangle$ is the input to the function and $\mathbf{W}_1, \mathbf{W}_2, \dots, \mathbf{W}_L$ are the unitary operations at each layer consisting of tensor products of 2-local unitary operators acting on neighboring qubits. Then, the concept class \mathcal{H} has SQ dimension $\text{SQ-DIM}_{\mathcal{D}}(\mathcal{H}) \geq 4^{\min(2L, n)} - 1$ under any distribution of states that forms a 2-design.

Proof. Our proof relies on the fact that with L layers, one can conjugate the fixed single qubit measurement on qubit m to produce any $2L$ -qubit Pauli on the $2L$ qubits within the reverse light cone of m . We follow a proof outline similar to Proposition C.4.

Before we proceed, we assume without loss of generality, that L is odd and the first layer applies a two qubit unitary to qubit m and the preceding qubit $m - 1$. It is straightforward to extend this to the case where L is even. Therefore, qubit m is the L -th qubit in the reverse light cone of qubit m , i.e., the light cone traverses qubits $m - L$ to $m + L - 1$. For the steps below, we then index the qubits from $-L$ to $L - 1$ so that the numbering is relative to qubit m . To perform a given $2L$ Pauli operator $\mathbf{P}_{-L} \otimes \mathbf{P}_{-L+1} \otimes \dots \otimes \mathbf{P}_{L-1}$ in the reverse light cone of qubit m , we follow the steps below, many of which are copied from Proposition C.4.:

1. In the first layer, apply a unitary to each qubit i which maps the computational basis to the basis of the Pauli for qubit i . In more detail, if $\mathbf{P}_i = \mathbf{I}$ or $\mathbf{P}_i = \mathbf{Z}$, then apply the identity map to keep the basis the same. If $\mathbf{P}_i = \mathbf{X}$, then apply the Hadamard transform and if $\mathbf{P}_i = \mathbf{Y}$ then apply the operation $\mathbf{H}\sqrt{\mathbf{Z}}^\dagger$.
2. in the L -th layer, for the 2-qubit unitary acting on qubits 0 and -1 , apply the following gate:
 - if all of $\mathbf{P}_{-L}, \mathbf{P}_{-L+1}, \dots, \mathbf{P}_{-1}$ are equal to \mathbf{I} and all of $\mathbf{P}_1, \mathbf{P}_2, \dots, \mathbf{P}_{L-1}$ are equal to \mathbf{I} , then apply the identity.
 - if any of $\mathbf{P}_{-L}, \mathbf{P}_{-L+1}, \dots, \mathbf{P}_{-1}$ are not equal to \mathbf{I} and any of $\mathbf{P}_1, \mathbf{P}_2, \dots, \mathbf{P}_{L-1}$ are not equal to \mathbf{I} , apply the following 2-qubit gate (CNOT) to i and $i + 1$ which conjugates $\mathbf{I} \otimes \mathbf{Z}$ to $\mathbf{Z} \otimes \mathbf{Z}$:

$$\begin{bmatrix} 1 & 0 & 0 & 0 \\ 0 & 1 & 0 & 0 \\ 0 & 0 & 0 & 1 \\ 0 & 0 & 1 & 0 \end{bmatrix}. \quad (\text{C.17})$$

- otherwise, apply the swap operation between qubits 0 and -1 .

3. In the l -th layer for any $l \neq L$, apply a specific two qubit gate to neighboring qubit pairs $\{-L + l - 1, -L + l\}$ on the edge of the reverse light cone. For simplicity, let $i = -L + 1 - 1$ and apply the following gate to qubit pair $\{i, i + 1\}$:

- if all of $\mathbf{P}_{-L}, \mathbf{P}_{-L+1}, \dots, \mathbf{P}_i$ are equal to \mathbf{I} , then apply the identity.
- if any of $\mathbf{P}_{-L}, \mathbf{P}_{-L+1}, \dots, \mathbf{P}_i$ are not equal to \mathbf{I} and $\mathbf{P}_{i+1} = \mathbf{I}$, then apply a swap between qubits i and $i + 1$.
- otherwise, apply the following 2-qubit gate (CNOT) to i and $i + 1$ which conjugates $\mathbf{I} \otimes \mathbf{Z}$ to $\mathbf{Z} \otimes \mathbf{Z}$:

$$\begin{bmatrix} 1 & 0 & 0 & 0 \\ 0 & 1 & 0 & 0 \\ 0 & 0 & 0 & 1 \\ 0 & 0 & 1 & 0 \end{bmatrix}. \quad (\text{C.18})$$

Similarly, for the other edge of the reverse light cone, we apply the same gates, but in “reverse” logic. Here, we apply a 2-qubit unitary to qubit pair $\{L - l - 2, L - l - 1\}$. For simplicity, let $i = L - l - 2$ and apply the following gate to qubit pair $\{i, i + 1\}$:

- if all of $\mathbf{P}_{i+1}, \mathbf{P}_{i+2}, \dots, \mathbf{P}_{L-1}$ are equal to \mathbf{I} , then apply the identity.
- if any of $\mathbf{P}_{i+1}, \mathbf{P}_{i+2}, \dots, \mathbf{P}_{L-1}$ are not equal to \mathbf{I} and $\mathbf{P}_{i+1} = \mathbf{I}$, then apply a swap between qubits i and $i + 1$.

- otherwise, apply the following 2-qubit gate to i and $i + 1$ which conjugates $\mathbf{Z} \otimes \mathbf{I}$ to $\mathbf{Z} \otimes \mathbf{Z}$:

$$\begin{bmatrix} 1 & 0 & 0 & 0 \\ 0 & 0 & 0 & 1 \\ 0 & 0 & 1 & 0 \\ 0 & 1 & 0 & 0 \end{bmatrix}. \quad (\text{C.19})$$

4. repeat step 3 above starting from $l = 1$ to $l = L - 1$. Measuring the m -th qubit will measure the corresponding desired Pauli. Note, that the single qubit operations of step 1 and the two-qubit operations of step 2 can be combined into a single 2-qubit gate thus not changing the depth.

□

Corollary C.7. *By application of Theorem 3.3, the class of functions defined in Proposition C.6 consisting of L layers of neighboring 2-qubit gates and a fixed measurement on a single qubit requires $2^{\Omega(\min(2L, n))}$ queries to learn for a constant query tolerance that does not depend on L and n .*

The above can be generalized to lower bound the statistical query dimension for circuits of L layers on d -dimensional lattices as we show below. In d -dimensional lattices, since the light cone of a single qubit measurement grows at a rate of L^d for an L layers, we can prove that the statistical query dimension grows as $2^{\Omega(\min(2L, n^{1/d})^d)}$.

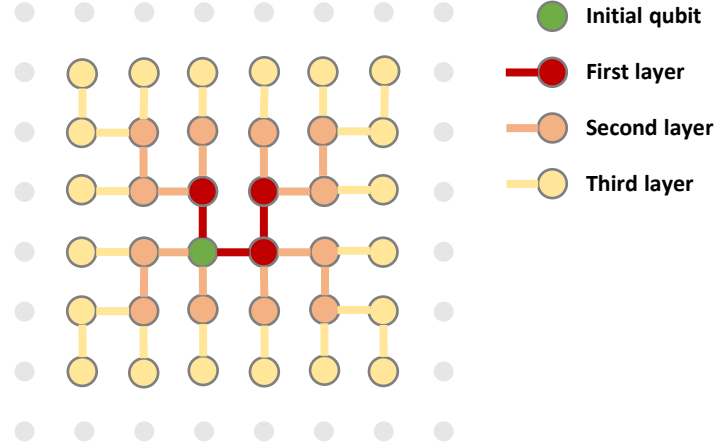


Figure 6: Growth of the light cone for a 2-dimensional lattice, where the initial qubit is the one that is measured. The size of the lattice grows with the perimeter of the light cone for each layer which consists of local 2-qubit gates applied in each dimension. Each qubit is connected to a qubit in the edge of the light cone of the prior layer, forming a graph which is a tree rooted at the initial qubit.

Proposition C.8 (SQ dimension for L layers, neighboring 2-local gates on d -dimensional lattice and fixed single qubit measurement). *Given n qubits, let \mathcal{H} be the concept class containing functions $f : \mathbb{C}^{2^n} \rightarrow \mathbb{R}$ consisting of L layers of 2-qubit unitary operations applied in each dimension followed by a Pauli Z measurement on a single qubit (labeled qubit m), i.e. functions of the form*

$$f(|\psi\rangle; \mathbf{W}_1, \mathbf{W}_2, \dots, \mathbf{W}_L) = \langle \psi | \mathbf{W}_1^\dagger \mathbf{W}_2^\dagger \cdots \mathbf{W}_L^\dagger (\mathbf{Z}_m) \mathbf{W}_L \cdots \mathbf{W}_2 \mathbf{W}_1 | \psi \rangle, \quad (\text{C.20})$$

where $|\psi\rangle$ is the input to the function and $\mathbf{W}_1, \mathbf{W}_2, \dots, \mathbf{W}_L$ are the unitary operations at each layer consisting of tensor products of 2-local unitary operators acting along each dimension on neighboring qubits in a d -dimensional lattice. Then, the concept class \mathcal{H} has SQ dimension $\text{SQ-DIM}_{\mathcal{D}}(\mathcal{H}) = 2^{\Omega(\min(2L, n^{1/d})^d)}$ under any distribution of states that forms a 2-design.

Proof. Our proof relies on the fact that with L layers, one can conjugate the fixed single qubit measurement on qubit m to produce any Pauli on the $\Omega(L^d)$ qubits within the reverse light cone of m . We follow a proof outline similar to Proposition C.6.

To be more precise, let us introduce some notation. To perform any Pauli measurement in the reverse light cone at a given layer $l \in [L]$ indexed in reverse order, we apply gates to the perimeter of the reverse light cone at layer $l - 1$. We assume there are N_l qubits in the reverse light cone at layer l and index these qubits from 1 to N_l to construct the Pauli $\mathbf{P}_1 \otimes \mathbf{P}_2 \otimes \dots \otimes \mathbf{P}_{N_l}$. Like in Proposition C.6, we grow the Pauli at each layer.

To grow the light cone and properly choose the 2-qubit gates, we construct a graph which is a tree where the parent of any qubit is the prior qubit which it was connected to in the light cone of the previous layer (see Figure 6 for an example). The root of the tree is the qubit which is being measured. For example, at layer $l = 1$, the light cone is of size two in each dimension and the qubit being measured is the parent to the child node which it is connected to. To construct any pauli $\mathbf{P}_1 \otimes \mathbf{P}_2 \otimes \dots \otimes \mathbf{P}_{N_L}$, we follow the steps below:

1. in the l -th layer, for all parent and child qubits p and c respectively connected in the tree at layer l , apply a unitary acting on qubits p and c as follows:

- if all of the qubits that are descendants of qubit c and qubit c itself have Pauli terms that are equal to \mathbf{I} , then apply the identity gate between qubit p and c .
- if any of the qubits that are descendants of qubit c or qubit c itself have Pauli terms that are not equal to \mathbf{I} and the Pauli term of qubit p is equal to \mathbf{I} , then apply the swap gate between p and c .
- otherwise, apply the following 2-qubit gate to qubits p and c which conjugates $\mathbf{Z} \otimes \mathbf{I}$ to $\mathbf{Z} \otimes \mathbf{Z}$:

$$\begin{bmatrix} 1 & 0 & 0 & 0 \\ 0 & 0 & 0 & 1 \\ 0 & 0 & 1 & 0 \\ 0 & 1 & 0 & 0 \end{bmatrix}. \quad (\text{C.21})$$

2. repeat the step above starting from $l = 1$ to $l = L$.
3. In the first layer ($l = L$), apply a unitary to each qubit i which maps the computational basis to the basis of the Pauli for qubit i . In more detail, if $\mathbf{P}_i = \mathbf{I}$ or $\mathbf{P}_i = \mathbf{Z}$, then apply the identity map to keep the basis the same. If $\mathbf{P}_i = \mathbf{X}$, then apply the Hadamard transform and if $\mathbf{P}_i = \mathbf{Y}$ then apply the operation $\mathbf{H}\sqrt{\mathbf{Z}}^\dagger$.

Following the above steps, measuring the single qubit will measure the corresponding desired Pauli. Note, that the single qubit operations of the first layer and the two-qubit operations of that layer can be combined into a single 2-qubit gate thus not changing the depth.

In each layer, 2-qubit gates act along each dimension in some order. We can assume an ordering of the dimensions without loss of generality and assume that we apply gates along that dimension in order. After the first layer, the lattice has size 2 along each dimension. For each layer thereafter, the lattice grows by 2 qubits in each dimension (see Figure 6 for example). Therefore, the reverse light cone grows at a rate $\Omega(L^d)$. Since the light cone can be at most of size n (number of qubits), then the light cone is of size $2^{\Omega(\min(2L, n^{1/d})^d)}$ for all L layers. \square

Corollary C.9. *By application of Theorem 3.3, the class of functions defined in Proposition C.8 consisting of L layers of neighboring 2-qubit gates and a fixed measurement on a single qubit requires $2^{\Omega(\min(2L, n^{1/d})^d)}$*

queries to learn for a query tolerance that decays no faster than $2^{\omega(\min(2L, n^{1/d})^d)}$. For $L \ll n$, this is equal to $2^{\Omega(L^d)}$ for any constant query tolerance that does not depend on L or n .

Proposition C.10 (SQ dimension for $L = 1$, unitary compiling, and single qubit gates). *Given n qubits, let \mathcal{H} be the concept class containing unitary transformations $\mathbf{V} : \mathbb{C}^{2^n} \rightarrow \mathbb{C}^{2^n}$ consisting of single qubit rotations in a single layer*

$$\mathbf{V}(|\psi\rangle, \mathbf{U}_1, \mathbf{U}_2, \dots, \mathbf{U}_n) = \mathbf{U}_1 \otimes \mathbf{U}_2 \otimes \dots \otimes \mathbf{U}_n |\psi\rangle, \quad (\text{C.22})$$

where $|\psi\rangle$ is the input to the transformation and $\mathbf{U}_1, \mathbf{U}_2, \dots, \mathbf{U}_n$ are the parameterized 1-qubit operations. Then, the concept class \mathcal{H} has SQ dimension $\text{SQ-DIM}_{\mathcal{D}}(\mathcal{H}) \geq 4^n$ under the qUSQ model and any distribution \mathcal{D} of inputs that is a 2-design.

Proof. From Lemma C.1, we have that $\langle \mathbf{U}, \mathbf{V} \rangle_{\mathcal{D}} = 2^{-n} \text{Re} [\text{Tr}(\mathbf{U}^\dagger \mathbf{V})]$. With one layer of single qubit unitary operations, any Pauli matrix can be constructed. Since $\text{Tr}(\mathbf{P}_1 \mathbf{P}_2) = 0$ for any two distinct Pauli matrices \mathbf{P}_1 and \mathbf{P}_2 , there are at least 4^n matrices in \mathcal{H} which are orthogonal under the inner product. \square

Corollary C.11. *By application of Theorem 3.3, the class of functions defined in Proposition C.10 consisting of a single layer of single qubit unitaries requires $2^{\Omega(n)}$ queries to learn for a query tolerance greater than $4^{-\beta n}$, where $\beta < 1/2 - \Omega(1)$.*

C.3 Swap Test via Statistical Queries

In the task of unitary compiling, one is given copies of states which are inputs and outputs of a target unitary transformation, and the goal is to learn the unitary transformation from those states. More formally, we aim to learn a unitary \mathbf{U}_* given a distribution over inputs or a dataset of m state pairs $\{|\phi_i\rangle, \mathbf{U}_* |\phi_i\rangle\}_{i \in [m]}$.

One means of measuring overlaps between states is via the swap test [16]. For pure states, $|\phi\rangle$ and $|\psi\rangle$, the swap test measures the fidelity $|\langle\phi|\psi\rangle|^2$. The measured register in the swap test outputs $|0\rangle$ with probability $1/2 + |\langle\phi|\psi\rangle|^2/2$ and $|1\rangle$ otherwise. As we show in the main text, this quantity can be calculated using queries to qUSQ. We use the helper lemma below to prove this fact.

Lemma C.12. *For any distribution \mathcal{D} that is a 2-design on a Hilbert space of dimension m ,*

$$\mathbb{E}_{\rho \sim \mathcal{D}} [\text{Tr}(\mathbf{U}_* \rho \mathbf{U}_*^\dagger \mathbf{V} \rho \mathbf{V}^\dagger)] = \frac{m^{-1} |\text{Tr}(\mathbf{V}^\dagger \mathbf{U}_*)|^2 + 1}{m + 1}. \quad (\text{C.23})$$

Proof. WLOG, we rewrite the equation above in terms of a distribution over pure states. Since mixed states are themselves distributions over pure states, this can always be done. Therefore, with a slight abuse of notation, we let \mathcal{D} also denote a distribution over unitary matrices \mathbf{U} that forms a 2-design:

$$\begin{aligned} \mathbb{E}_{\rho \sim \mathcal{D}} [\text{Tr}(\mathbf{U}_* \rho \mathbf{U}_*^\dagger \mathbf{V} \rho \mathbf{V}^\dagger)] &= \mathbb{E}_{\mathbf{U} \sim \mathcal{D}} [\langle 0 | \mathbf{U}^\dagger \mathbf{V}^\dagger \mathbf{U}_* \mathbf{U} | 0 \rangle \langle 0 | \mathbf{U}^\dagger \mathbf{U}_*^\dagger \mathbf{V} \mathbf{U} | 0 \rangle] \\ &= \mathbb{E}_{\mathbf{U} \sim \mathcal{D}} [\langle 0 | \mathbf{U}^\dagger \mathbf{V}^\dagger \mathbf{U}_* \mathbf{U} | 0 \rangle]^2. \end{aligned} \quad (\text{C.24})$$

Using equation C.1 and equation C.2, we have

$$\begin{aligned} \mathbb{E}_{\mathbf{U} \sim \mathcal{D}} [\langle 0 | \mathbf{U}^\dagger \mathbf{V}^\dagger \mathbf{U}_* \mathbf{U} | 0 \rangle]^2 &= \mathbb{E}_{\mathbf{U} \sim \mathcal{D}} [\langle 0 | \mathbf{U}^\dagger \mathbf{V}^\dagger \mathbf{U}_* \mathbf{U} | 0 \rangle \langle 0 | \mathbf{U}^\dagger \mathbf{U}_*^\dagger \mathbf{V} \mathbf{U} | 0 \rangle] \\ &= \mathbb{E}_{\mathbf{U} \sim \mathcal{D}} [\langle I_m^2 | ((\mathbf{V}^\dagger \mathbf{U}_*) \otimes (\mathbf{U}_*^\dagger \mathbf{V}) \otimes \mathbf{I} \otimes \mathbf{I}) (\mathbf{U} \otimes \mathbf{U} \otimes \bar{\mathbf{U}} \otimes \bar{\mathbf{U}}) | 0 \rangle^{\otimes 4}]. \end{aligned} \quad (\text{C.25})$$

Applying equation C.3, we have

$$\begin{aligned}
\mathbb{E}_{\mathbf{U} \sim \mathcal{D}} \left[\left| \langle 0 | \mathbf{U}^\dagger \mathbf{V}^\dagger \mathbf{U}_* \mathbf{U} | 0 \rangle \right|^2 \right] &= \frac{1}{m^2 - 1} \langle I_m^2 | ((\mathbf{V}^\dagger \mathbf{U}_*) \otimes (\mathbf{U}_*^\dagger \mathbf{V}) \otimes \mathbf{I} \otimes \mathbf{I}) \left(|I_m^2\rangle \langle I_m^2| + |S_m^2\rangle \langle S_m^2| \right) |0\rangle^{\otimes 4} \\
&\quad - \frac{1}{m(m^2 - 1)} \langle I_m^2 | ((\mathbf{V}^\dagger \mathbf{U}_*) \otimes (\mathbf{U}_*^\dagger \mathbf{V}) \otimes \mathbf{I} \otimes \mathbf{I}) \left(|I_m^2\rangle \langle S_m^2| + |S_m^2\rangle \langle I_m^2| \right) |0\rangle^{\otimes 4} \\
&= \frac{1}{m^2 - 1} (\text{Tr}[\mathbf{V}^\dagger \mathbf{U}_*] \text{Tr}[\mathbf{U}_*^\dagger \mathbf{V}] + \text{Tr}[\mathbf{V}^\dagger \mathbf{U}_* \mathbf{U}_*^\dagger \mathbf{V}]) \\
&\quad - \frac{1}{m(m^2 - 1)} (\text{Tr}[\mathbf{V}^\dagger \mathbf{U}_*] \text{Tr}[\mathbf{U}_*^\dagger \mathbf{V}] + \text{Tr}[\mathbf{V}^\dagger \mathbf{U}_* \mathbf{U}_*^\dagger \mathbf{V}]) \\
&= \left(\frac{1}{m^2 - 1} - \frac{1}{m(m^2 - 1)} \right) \left(|\text{Tr}[\mathbf{V}^\dagger \mathbf{U}_*]|^2 + m \right) \\
&= \frac{m^{-1} |\text{Tr}[\mathbf{V}^\dagger \mathbf{U}_*]|^2 + 1}{m + 1}.
\end{aligned} \tag{C.26}$$

□

D Shallow VQAs Converge in Distribution to WHRFs

As discussed informally in Section 4.1, our goal is to demonstrate that certain distributions of shallow variational quantum algorithms (VQAs) weakly converge to Wishart hypertoroidal random fields (WHRFs). The distribution of local minima of WHRFs was shown in [5] to exhibit a phase transition in trainability, where *underparameterized models* are untrainable due to poor local minima, and *overparameterized models* exhibit local minima close to the global minimum (though may still be untrainable for other reasons, e.g. due to barren plateaus [60, 19, 63]).

Unlike the nonlocal ansatz case [5], here we are unable to show the full convergence in distribution of shallow local VQAs to WHRFs. Instead, we focus on the joint distribution of the loss function, gradient norm, and Hessian determinant, where the gradient and Hessian have been normalized by the number of parameters q in the reverse light cone of each term in the Pauli expansion of the problem Hamiltonian; by the parameter shift rule [70, 58], it is easy to see that this bounds the gradient norm and Hessian eigenvalues as q is large. The local minima results of [5] depend only on this joint distribution, and thus showing this convergence suffices for our purposes.

We now review the setup of the VQA loss functions we are considering. Throughout the course of this review, we will make various assumptions, particularly on the distribution of gates in the VQA ansatz and on the independence of various reverse light cones; we discuss these assumptions and whether or not they are reasonable in more detail at the end of this Appendix. As mentioned in Section 4.1, we consider optimizing VQAs on the problem Hamiltonian $\mathbf{H} \neq \mathbf{0}$, which has Pauli decomposition:

$$\mathbf{H} = \sum_{i=1}^A \alpha_i \mathbf{P}_i. \tag{D.1}$$

WLOG, we assume here \mathbf{H} is traceless, and that all $\alpha_i > 0$. To simplify our analysis, we will consider the case where the reverse light cone of each term $\alpha_i \mathbf{P}_i$ in the Pauli decomposition of \mathbf{H} is i.i.d. drawn from the same distribution of ansatzes, with the same parameter dependence. To make this more concrete, assume that the reverse light cone of each $\alpha_i \mathbf{P}_i$ is of the form $\mathbf{V}_i(\boldsymbol{\theta}) |0\rangle$ where $\boldsymbol{\theta} \in \mathbb{R}^q$, and has support on a number $l \ll n$ of qubits. In this regime, we can scale and shift the loss landscape of equation 5 to be of the form:

$$F_{\text{VQE}}(\boldsymbol{\theta}) = 1 - \lambda_0^{-1} \sum_{i=1}^A \alpha_i \langle \mathbf{0} | \mathbf{V}_i(\boldsymbol{\theta})^\dagger \mathbf{P}_i \mathbf{V}_i(\boldsymbol{\theta}) | \mathbf{0} \rangle = 1 + \|\boldsymbol{\alpha}\|_1^{-1} \sum_{i=1}^A \alpha_i \langle \mathbf{0} | \mathbf{V}_i^\dagger(\boldsymbol{\theta}) \mathbf{P}_i \mathbf{V}_i(\boldsymbol{\theta}) | \mathbf{0} \rangle, \tag{D.2}$$

where λ_0 is the ground state energy of \mathbf{H} and $\boldsymbol{\alpha}$ is the vector of all α_i .

We assume that $\mathbf{V}_i(\boldsymbol{\theta})$ is of the form:

$$\mathbf{V}_i(\boldsymbol{\theta}) = \mathbf{W}_i(\boldsymbol{\theta}) \mathbf{U}_i, \quad (\text{D.3})$$

where \mathbf{U}_i are i.i.d. drawn from an ϵ -approximate t -design under the monomial measure on l qubits [40], where $\epsilon = O(1)$. Note that in particular, though the total ansatz size n may be large, all potential scrambling of the ansatz may only happen locally, in regions of size $l \ll n$; in other words, these ansatzes are *not* expected to suffer from barren plateaus, particularly if $l = O(\log(n))$ [19, 63]. \mathbf{W}_i is composed of fixed parameterized rotations which we take WLOG to be of the form $\mathbf{R}_{\mathbf{Y}_a}(\theta_b) = \exp(-i\theta_b \mathbf{Y}_a)$ (where as previously mentioned, this parameter dependence is identical across all \mathbf{W}_i), fixed gates, and potentially randomly chosen gates such that \mathbf{W}_i itself is a random field. For simplicity, we also assume that all θ_i are independent from one another (i.e. we are in the $r = 1$ regime of [5]), and that each qubit in the reverse light cone has at least one parameterized gate. We also assume that the field $\mathbf{W}_i(\boldsymbol{\theta})$ is rotationally invariant in θ_i .

We now give the formal statement and proof of Theorem 4.1. First, the formal statement:

Theorem D.1 (Approximately locally scrambled variational loss functions converge to WHRFs). *Let $p_{VQE,\boldsymbol{\theta}}$ be the joint distribution of the loss function of equation D.2, its gradient norm, and the determinant of its Hessian at $\boldsymbol{\theta}$, where the gradient and Hessian are normalized by q . Let $p_{WHRF,\boldsymbol{\theta}}$ be the same for the WHRF:*

$$F_{WHRF}(\boldsymbol{\theta}) = m^{-1} \sum_{i,j=1}^{2^l} w_i J_{i,j} w_j \quad (\text{D.4})$$

with $m = \frac{\|\boldsymbol{\alpha}\|_1^2}{\|\boldsymbol{\alpha}\|_2^2} 2^{l-1}$ degrees of freedom, where $\mathbf{J} \sim \mathcal{CW}_{2^l}(m, \mathbf{I}_{2^l})$. Here, \mathbf{w} are points on the hypertorus $(S^1)^{\times l}$ parameterized by $\tilde{\boldsymbol{\theta}}$, where $\tilde{\theta}_i$ is the sum of all θ_j on qubit i . We then have that $p_{VQE,\boldsymbol{\theta}}$ weakly converges to $p_{WHRF,\boldsymbol{\theta}}$, up to an error $\tilde{O}(\text{poly}(\frac{1}{t} + \epsilon + \exp(-l)))$ in Lévy–Prokhorov distance.

As we previously mentioned, for technical reasons, we only prove the convergence of the joint distribution of the loss and certain functions of its first two derivatives. We emphasize once more that this does not affect our final conclusions, as all results on the local minima distribution of WHRFs given in [5] depend only on this joint distribution.

To prove Theorem D.1, we begin by showing that, up to terms that go to zero polynomially quickly as $\epsilon \rightarrow 0, t \rightarrow \infty$, one can WLOG consider ansatzes of the form of equation D.2 that are explicitly Haar random within each reverse light cone of size l .

Lemma D.2 (Approximate local scrambling bound on the loss function and its derivatives). *Let $p_{VQE,\boldsymbol{\theta}}$ be the joint distribution described in Theorem D.1. Let $p_{Haar,\boldsymbol{\theta}}$ be the same, for \mathbf{U}_i taken to be i.i.d. Haar random. We then have that $p_{VQE,\boldsymbol{\theta}}$ weakly converges to $p_{Haar,\boldsymbol{\theta}}$, up to an error $\tilde{O}(\text{poly}(\frac{1}{t} + \epsilon))$ in Lévy–Prokhorov distance.*

Proof. Let $\phi_{VQE}(\mathbf{x} \mid \boldsymbol{\theta})$ be the joint characteristic function of $p_{VQE,\boldsymbol{\theta}}$, and similarly $\phi_{Haar}(\mathbf{x} \mid \boldsymbol{\theta})$. Since \mathbf{U}_i are assumed to be i.i.d. ϵ -approximate t -designs under the monomial measure, for any moments $M_{VQE,\boldsymbol{\theta}}, M_{Haar,\boldsymbol{\theta}}$ of degree s of $p_{VQE,\boldsymbol{\theta}}, p_{Haar,\boldsymbol{\theta}}$, respectively, we have that:

$$|M_{VQE,\boldsymbol{\theta}} - M_{Haar,\boldsymbol{\theta}}| = O(\epsilon \mathbf{1}[s \leq t] + \mathbf{1}[s > t]). \quad (\text{D.5})$$

In particular, for all T sublinear in t ,

$$|\phi_{VQE}(\mathbf{x} \mid \boldsymbol{\theta}) - \phi_{Haar}(\mathbf{x} \mid \boldsymbol{\theta})| = O\left(\epsilon \text{poly}(T) + \frac{(3T)^t}{t!}\right) \quad (\text{D.6})$$

for all \mathbf{x} with $\|\mathbf{x}\|_\infty \leq T$. Similar inequalities hold for the partial derivatives of the joint characteristic functions. Therefore, there exists some $T = \Omega(\text{poly}(\min(t, \frac{1}{\epsilon})))$ such that the second bound of Theorem 4 of [82] (with $m = \log(T)$) on the Lévy–Prokhorov distance is $\tilde{O}(\text{poly}(\frac{1}{t} + \epsilon))$. \square

Until now, we have considered ansatzes with generic parameter dependence. We now show that up to terms vanishing exponentially quickly in the reverse light cone size l , we can consider a canonical ansatz form WLOG.

Lemma D.3 (Canonical form for Hamiltonian agnostic variational loss functions). *Let $p_{\text{Haar},\theta}$ be the joint distribution described in Lemma D.2. Let $p_{\text{can},\theta}$ be the same for the variational loss function*

$$F_{\text{can}}(\theta) = \|\alpha\|_1^{-1} \sum_{i=1}^A \alpha_i \langle \mathbf{0} | \mathbf{R}(\theta)^\dagger \mathbf{U}_i^\dagger \mathbf{P}_i \mathbf{U}_i \mathbf{R}(\theta) | \mathbf{0} \rangle + 1, \quad (\text{D.7})$$

where $\mathbf{R}(\theta)$ is the product of the parameterized rotations of equation D.3. We then have that $p_{\text{Haar},\theta}$ weakly converges to $p_{\text{can},\theta}$, up to an error $\tilde{O}(\text{poly exp}(-l))$ in Lévy–Prokhorov distance.

Proof. Let us consider (generally mixed) moments involving random variables of the form:

$$K_{ij}(\theta_j) = \langle \mathbf{0} | \mathbf{U}_i^\dagger \mathbf{W}_i(\theta_j)^\dagger \mathbf{P}_i \mathbf{W}_i(\theta_j) \mathbf{U}_i | \mathbf{0} \rangle - \langle \mathbf{0} | \tilde{\mathbf{U}}_{ij}^\dagger \mathbf{U}_i^\dagger \mathbf{W}_i(\theta_j)^\dagger \mathbf{P}_i \mathbf{W}_i(\theta_j) \mathbf{U}_i \tilde{\mathbf{U}}_{ij} | \mathbf{0} \rangle, \quad (\text{D.8})$$

where $\mathbf{U}_i, \tilde{\mathbf{U}}_{ij}$ are i.i.d. Haar random on l qubits. By the asymptotic free independence of Haar random matrices from constant matrices, and the fact that

$$\text{tr} \left(\mathbf{W}_i(\theta_j) \mathbf{P}_i \mathbf{W}_i(\theta_j)^\dagger \right) = \text{tr} \left(| \mathbf{0} \rangle \langle \mathbf{0} | - \tilde{\mathbf{U}}_{ij}^\dagger | \mathbf{0} \rangle \langle \mathbf{0} | \tilde{\mathbf{U}}_{ij} \right) = 0, \quad (\text{D.9})$$

we have that any such moment is on the order of $O(\text{poly exp}(-l))$ [77]. In particular, it is easy to see that up to an error in Lévy–Prokhorov distance on this order, one can WLOG take $p_{\text{can},\theta}$ as if the gradient and Hessian components had i.i.d. \mathbf{U}_{ij} rather than \mathbf{U}_i —for instance, this follows identically to the proof of Lemma D.2 with $\epsilon = O(\text{poly exp}(-l))$. The result then follows from the unitary invariance of the Haar measure. \square

We are now able to prove Theorem D.1, following essentially the same procedure as proving Theorem 5 of [5].

Proof. By Lemmas D.2 and D.3, $p_{\text{VQE},\theta}$ weakly converges to $p_{\text{Haar},\theta}$ up to an error $\tilde{O}(\text{poly}(\frac{1}{t} + \epsilon + \exp(-l)))$ in Lévy–Prokhorov distance. By Corollary 1 of [44], this then proves weak convergence of $p_{\text{VQE},\theta}$ to the corresponding joint distribution of a weighted sum of WHRFs each with 2^{l-1} degrees of freedom, up to an additional error in Lévy–Prokhorov distance exponentially small in l . Weak convergence to $p_{\text{WHRF},\theta}$ then follows from a trivial generalization of Theorem 5 of [5]. \square

Scope of results We now comment on the applicability of the results of [5] on the local minima distribution of WHRFs when Theorem D.1 holds. All analysis of the local minima distribution of WHRFs in [5] depends only on the joint distribution $p_{\text{WHRF},\theta}$, up to a change in normalization of the gradient and Hessian by l rather than q that does not contribute to the logarithmic asymptotics (i.e. Theorem 7 of [5]) when $q \log(q) = o(m)$. Thus, in the discussion of Section 4.1, we take this as an extra assumption. Furthermore, we note that the analysis of Section 4.1 holds only up to shifts on the order of $\tilde{O}(\text{poly}(\frac{1}{t} + \epsilon + \exp(-l)))$ in the joint distribution $p_{\text{WHRF},\theta}$, due to the rate of convergence of Theorem D.1. However, shifts on this order do not affect the conclusions of [5] for sufficiently large constant ϵ^{-1}, t .

Assumptions Let us now discuss in more detail the assumptions made in the course of proving Theorem D.1. First, we assume that at least some part of the ansatz circuit scrambles some local region around any measured observable; that is, we assume that the ansatz locally is an ϵ -approximate t design for sufficiently large ϵ^{-1}, t . It is known that shallow, local circuits dimensions exhibit this property, when 2-local Haar random gates are applied [40]; thus, in a practical sense, our results assume that the local gates in any distribution of ansatzes under consideration are approximately Haar random. This is a typical model of

Ansatz	Experiment	Figure	# Parameters	Optimizer	Learning Rate
QCNN	Teacher-Student	Figure 3	$16 \lceil \log_2 n \rceil = O(\log n)$	Adam	0.001
Checkerboard	Teacher-Student	Figure 4	$32L \lfloor \frac{n}{2} \rfloor = O(nL)$	Adam	0.001 (underparameterized)
	VQE (GD)	Figure 5a	$128 \lfloor \frac{n}{2} \rfloor = O(n)$	vanilla GD	0.001 (overparameterized)
	VQE (Adam)	Figure 10	$128 \lfloor \frac{n}{2} \rfloor = O(n)$	Adam	0.003
	Adaptive VQE	Figure 5b	$160L = O(L)$	Adam	0.002 (5% reduction each layer)

Table 3: List of parameter counts, optimizers, and learning rates for the various ansatzes and experiments. L denotes the number of layers and n the number of qubits.

Hamiltonian agnostic ansatzes, where the ansatz is chosen independently from the problem Hamiltonian \mathbf{H} ; see for instance the discussion in Section 2.2 and the references therein. The inapplicability of this assumption to *Hamiltonian informed ansatzes*—particularly for highly symmetric problems—is discussed in more detail in Appendix G, where we review models that may not suffer from the poor trainability properties we show here.

Our other major assumption is the independence of the $\mathbf{V}_i(\boldsymbol{\theta})$ (up to the repeated use of parameters). Of course, in practice this is almost never true, as otherwise variational optimization would proceed via optimizing each reverse light cone independently. However, given a problem Hamiltonian \mathbf{H} and a shallow ansatz, one can consider a subset of Pauli operators in the Pauli decomposition of \mathbf{H} such that their reverse light cones do not overlap. There is little reason to believe that the loss landscape of this simplified problem should be any more difficult to optimize over than the full problem. We therefore suspect that this assumption is little more than a technical requirement. A similar generalization one could consider is taking the parameters of each \mathbf{V}_i to being almost entirely independent of one another (though not entirely independent, as one could then optimize each subproblem independently, and n would no longer an accurate measure of the size of the problem). However, in this regime we expect the “effective” overparameterization ratio γ to go as $(\frac{L}{2^i})^A$, as the problem essentially reduces to simultaneously optimizing A loss functions. For $A \sim n$, for instance, this decays exponentially in n , and thus we believe that models of this form are also not trainable.

E Details of Numerical Experiments

All experiments were performed in Python using the Pytorch [65] package to perform automatic differentiation. Computation was performed on Nvidia RTX™ A6000 GPUs. Important hyperparameters for the experiments are listed in Table 3. Unless otherwise stated, all gradients were calculated using analytic formulas for automatic differentiation with computer precision (32 bit floating point). Therefore, issues with decaying gradients and barren plateaus do not appear in these simulations for the relatively small number of qubits considered. Gradient based optimization was performed using vanilla gradient descent or the Adam optimizer [52], a popular and effective algorithm for training deep neural networks. We tested other optimizers as well and found no noticeable difference in performance.

Loss surface plot (Figure 1) To generate this plot, we chart the loss landscape at initialization of training in the teacher-student setup of Section 5.1 for the 14 qubit QCNN circuit. The teacher and student circuit were both initialized as described in Appendix E.1.

The loss is plotted along two normalized directions of the parameter landscape. Normalization is applied individually to the 3 filters of the 14 qubit QCNN. We loosely follow the “filter-wise” normalization strategy of [55], where we first generate a random direction by drawing a value for each parameter from an i.i.d. standard normal distribution. Then, we divide values for the parameters in a given layer by the Frobenius norm of the matrix for the corresponding layer.

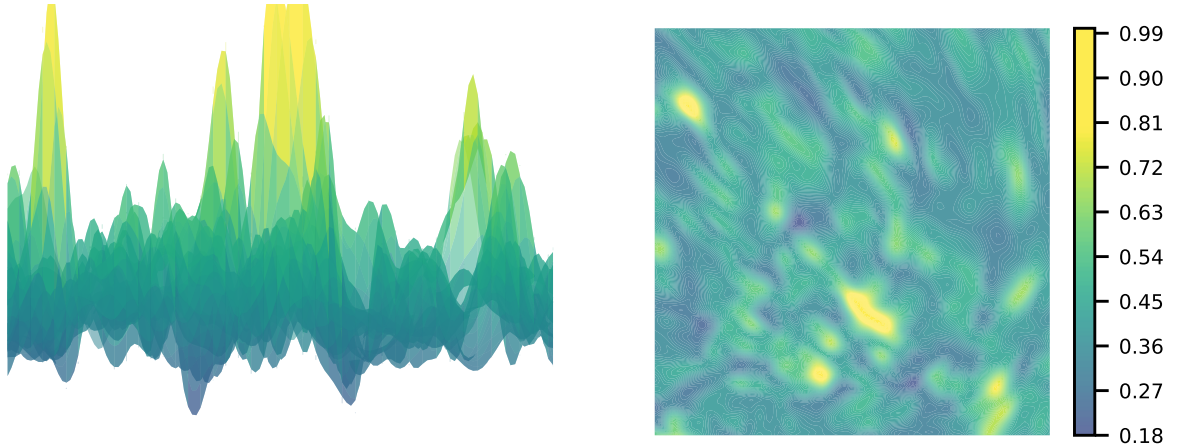


Figure 7: Loss landscape of the QCNN experiment replicated from Figure 1, except the initialization of the student circuit is randomly chosen. Here, the global minimum is likely far away and the landscape also appears “bumpy”; all local minima in the region considered here are far from the global optimum.

In Figure 1, we plot the mean squared error loss for the teacher-student task for a batch size of 128 randomly chosen computational basis states. The legend in the plot is shown relative to the maximum value of the loss in the range considered. A value of 0 here corresponds to the loss at the global minimum. The middle of the plot corresponds to the exact parameters of the teacher circuit, and hence, is a global minimum. This setting is, in a sense, an optimistic setting since initialization is near a global minimum. For comparison, we include in Figure 7 an example of a loss surface where the student circuit is not initialized near the parameters of the teacher circuit. As is evident in this setting, no longer is there a global minimum in the parameter region considered, and the landscape also appears to be filled with traps.

E.1 QCNN Experiments

The quantum convolutional neural network (QCNN) is an ansatz originally proposed in [28]. This ansatz features parameter sharing across gates in a single layer. The form of this circuit is provided in Figure 8. In our experiments, we use the same form of the 2-local ansatz as in [28] and also studied in [67]. Between convolutional layers, we include no controlled unitary operations based on the measurement outcomes. In learning settings, we fully parameterize the 2-local unitaries in the skew Hermitian basis of the unitary Lie algebra. To achieve this, we train directly over parameter entries of a matrix \mathbf{M} and apply $e^{\mathbf{H}}$, where $\mathbf{H} = \mathbf{M} - \mathbf{M}^\dagger$, to perform the resulting unitary transformation. Entries of the matrix \mathbf{M} were initialized i.i.d. from a standard normal distribution.

For the teacher-student experiments in Section 5.1, we aim to predict the outcome of the final green measurement depicted in Figure 8 for 512 randomly chosen computational basis states. For n qubits, the QCNN ansatz for both the teacher and student circuits have $16\lceil\log_2 n\rceil$ parameters which is a relatively small number compared to the dimension of the Hilbert space. All networks were trained for 5000 epochs and a learning rate of 0.001 using the Adam optimizer.

E.2 Checkerboard Ansatz

The checkerboard circuit applies gates in a one-dimensional lattice as shown in Figure 9. As in the QCNN experiments, we train directly over parameter entries of a matrix \mathbf{M} and apply $e^{\mathbf{H}}$, where $\mathbf{H} = \mathbf{M} - \mathbf{M}^\dagger$, to

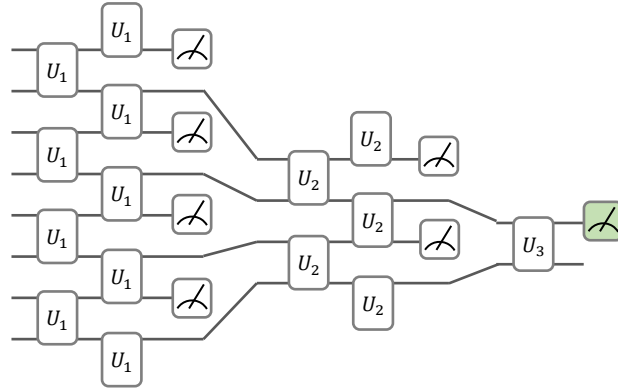


Figure 8: Circuit drawing of QCNN ansatz for 8 qubits. Layers of shared 2-local unitary transformations are applied followed by measurement of every other qubit. Gates at the edge of the circuit above are applied in a cyclic fashion (i.e. the top and bottom qubit interact). The measurement colored in green is the measurement outcome whose probability we aim to predict in the teacher-student setup. Generically for n qubits, this ansatz has depth $\lceil \log_2 n \rceil$. During training, the 2-local unitaries are fully parameterized for our simulations.

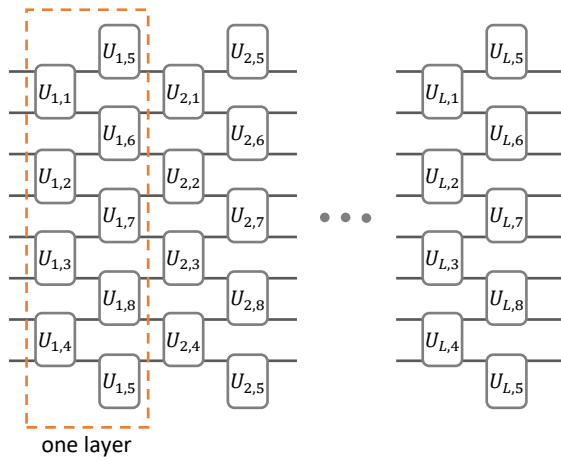


Figure 9: Circuit drawing of the checkerboard ansatz for 8 qubits and L layers. Gates at the edge of the circuit above are applied in a cyclic fashion (i.e. the top and bottom qubit interact). Generically for n qubits, this ansatz has $32L\lfloor n/2 \rfloor$ parameters. During training, the 2-local unitaries are fully parameterized for our simulations.

perform the resulting unitary transformation. Since the exponential map from the Lie algebra is surjective onto the unitary group, this parameterization is capable of expressing any unitary matrix. Entries of the matrix \mathbf{M} were initialized i.i.d. from a standard normal distribution.

For the teacher-student simulations (Figure 4), we train networks over 512 randomly chosen computational basis states which is more than the dimension of the Hilbert space and enough information to recover the full unitary transformation. Optimization was performed using the Adam optimizer and a batch size of 128. Networks were trained for 5000 epochs and training was stopped if the loss fell below 0.001 which only occurred for the overparameterized setting. We observed that for fewer than 8 qubits, training was successful with very small probability in the underparameterized setting.

E.3 VQE Experiments

For all of our VQE experiments, the target Hamiltonian \mathbf{H}_t was constructed by conjugating a local Hamiltonian of n qubits equal to $\sum_{i=1}^n \mathbf{Z}_i$ with alternating layers of products of two-qubit unitaries \mathbf{U}_1 and \mathbf{U}_2 . That is, \mathbf{H}_t takes the form below as copied from the main text:

$$\mathbf{H}_t = (\mathbf{U}_2^\dagger \mathbf{U}_1^\dagger)^L \left[\sum_{i=1}^n \mathbf{Z}_i \right] (\mathbf{U}_1 \mathbf{U}_2)^L + n\mathbf{I}. \quad (\text{E.1})$$

\mathbf{U}_1 and \mathbf{U}_2 are the tensor product of two-qubit unitaries which for n even take the form:

$$\begin{aligned} \mathbf{U}_1 &= \mathbf{U}_1^{(1,2)} \otimes \mathbf{U}_1^{(3,4)} \otimes \cdots \otimes \mathbf{U}_1^{(n-1,n)} \\ \mathbf{U}_2 &= \mathbf{U}_2^{(2,3)} \otimes \mathbf{U}_2^{(4,5)} \otimes \cdots \otimes \mathbf{U}_2^{(n,n+1)}, \end{aligned} \quad (\text{E.2})$$

where superscripts above indicate the pair of qubits each 2-local unitary acts on and indexing is taken mod n . Each 2 local unitary is drawn from the distribution $e^{\mathbf{H}}$, where $\mathbf{H} = \mathbf{G} - \mathbf{G}^\dagger$, and each \mathbf{G} is a 4×4 matrix with entries drawn i.i.d. from a random normal distribution. Trained unitaries in the checkerboard ansatz are also initialized in this fashion. Optimization is then performed directly on the entries of the matrix in the Lie algebra which form a complete basis for all of the 2-local unitaries.

In Figure 5a, each VQE instance was optimized for 30000 steps using a vanilla gradient descent optimizer with a learning rate of 0.01. For completeness, we replicate this plot with the Adam optimizer in Figure 10 and unsurprisingly observe similar convergence results. All calculations were performed to computer precision, which provides a best-case setting for optimization via real quantum hardware, since gradients and loss function values would have to be calculated using less precise sampling methods on actual quantum computers. In Figure 5b, optimization is performed using an adaptive VQE algorithm similar to the one in [38]. Here, a checkerboard ansatz is initialized as a single layer and optimization is performed layer-wise. We set $n = 11$ and small enough such that it is computationally feasible to overparameterize the ansatz. Each 5000 steps of optimization, a layer is added to the ansatz and initialized to the identity mapping. Each additional layer adds 160 trainable parameters to the ansatz. After each layer is added, the learning rate is multiplied by 0.95 to make the training more stable with more parameters. At each point in time, all parameters of the ansatz across all layers are trained. For aesthetic purposes and to see the course of training without significant jumps in the plot, we plot a moving average of the values across 10 sequential datapoints in Figure 5b.

F Untrainability Beyond Gradient Descent

One may wish to avoid local minima by changing the loss function or performing more advanced versions of gradient-based optimizers. Here, we give heuristic reasons why these two adjustments will likely not fix any issues of untrainability.

First, we examine changes in the loss function. This is commonly done to avoid barren plateaus and make gradients easier to compute. Let us assume that $\mathcal{L}(\boldsymbol{\theta})$ is our original loss function (as a function of

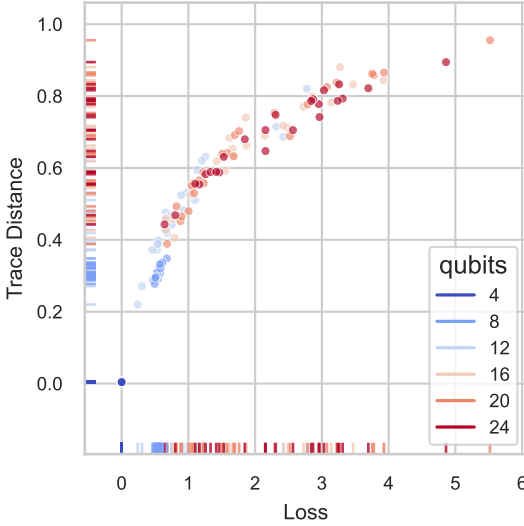


Figure 10: Scatter plot showing the values of the loss and trace distance of the final VQE state after 30000 steps of optimization using the Adam optimizer shows that the algorithm converges to poorer local minima as the number of qubits grows. Setting is replicated from Figure 5a with the sole change of the optimizer from gradient descent to Adam.

the parameters θ), which is changed to a new loss function $\tilde{\mathcal{L}}(\theta)$. Typically, $\tilde{\mathcal{L}}(\theta)$ is chosen so that it upper and lower bounds $\mathcal{L}(\theta)$, i.e. $C\tilde{\mathcal{L}}(\theta) \leq \mathcal{L}(\theta) \leq D\tilde{\mathcal{L}}(\theta)$ for some constants C, D . This guarantees convergence in both metrics when changing the loss function and is the case for e.g. local versions of the inner product and the quantum earth mover's (EM) distance [29, 47]. Now, let us assume that every continuous path from a local minimum at θ_l to the global minimum θ^* must increase the loss function by a factor $M > D/C$, i.e. there exists a point in the path that has value at least $M\mathcal{L}(\theta_l)$. Then, in the new loss function $\tilde{\mathcal{L}}(\theta_l) \leq \mathcal{L}(\theta_l)/C$. Furthermore, at some point in any continuous path, $\mathcal{L}(\theta) > M\mathcal{L}(\theta_l)$ which implies that at that point $\tilde{\mathcal{L}}(\theta) \geq \mathcal{L}(\theta)/D > M\mathcal{L}(\theta_l)/D = \mathcal{L}(\theta_l)/C$. Thus, θ_l is not within a convex region around the global optimum. This may be too restrictive of an assumption since local minima can often be very shallow, but it also seems to be backed by experiments.

Second, we consider changing the optimization algorithm to a second order optimization algorithm such as in [74]. These algorithms perform gradient descent by applying a transformation to the gradient of the form:

$$\theta_{t+1} = \theta_t - \mu \Sigma^+ \nabla_{\theta} \mathcal{L}(\theta_t), \quad (\text{F.1})$$

where Σ incorporates our second order term, e.g. the Hessian or Fubini–Study metric tensor, and Σ^+ is its pseudoinverse. Clearly, in the above, this does not allow one to escape a local minima. Setting $\theta_t = \theta^*$ above sets the gradient term to zero, and one again one is stuck in a local minimum.

Though other training methods exist, it is not clear *a priori* why they should succeed. For example, training in a layer-wise fashion also does not work as [47, 73, 17] show. Finally, note that the above methods can be very effective at alleviating barren plateaus. In fact, changes in metric and second order optimization methods are often precisely designed to fix this issue. Nevertheless, these methods only provably converge to the global optimum in convex or close to convex settings, which is not the case for essentially all variational quantum models.

G Potentially Trainable Variational Quantum Algorithms

As we discussed in Section 6, though our results imply that a wide swathe of variational quantum algorithms are not trainable, there still exist other classes of variational quantum algorithms that may be trainable. Indeed, it is known analytically that the quantum approximate optimization algorithm (QAOA) [33] is trainable due to *parameter concentration*, where the global optimum for small problem instances is close to the global optimum for large problem instances [15]. These results have been used to show that QAOA is able to outperform certain classical optimization algorithms for specified combinatorial optimization problems [34]. These results demonstrate the power of *good model initialization* in variational quantum algorithms; even if the total variational landscape is swamped with poor local minima, good initialization may ensure that the optimizer begins in the region of attraction of the global minimum. Though this is perhaps most relevant for the variational quantum eigensolver (VQE) [66] and QAOA [33], where there exists physical intuition for potentially performant parameter initializations, in more traditional machine learning settings this may manifest as good performance on certain inputs to the model.

Variationally studying models with many symmetries may also avoid our poor performance guarantees. Intuitively, both our results here and the results of [5] are consequences of either local or global, respectively, *underparameterization*. Namely, unless the ansatz is parameterized such that the number of parameters grows with the (local) Hilbert space dimension, the model is not trainable. Typically, this Hilbert space dimension is exponential in the problem size. However, if the model is heavily constrained by symmetries, this dimension might be much smaller. Indeed, such models were studied numerically in [53, 79], where it was shown that certain variational quantum algorithms optimize efficiently. Though often these models can be solved classically when the symmetries are known, these symmetries may not be known *a priori*. Indeed, one may be able to test for the presence of symmetries in a given model by studying whether associated variational quantum algorithms are trainable. Similar to these general symmetry considerations, known structure in the problem may also allow one to build up hierarchical ansatzes that are able to be trained sequentially. We leave further investigation in these directions to future work.

Finally, though most variational models fit the framework of equation 5, there exist other settings of variational quantum algorithms. One class of such models includes *quantum Boltzmann machines*, which attempt to model given quantum states via the training of quantum Gibbs states [3]. When the full quantum Gibbs state is observed, it is known that these models are efficiently trainable [6], and numerically it is known that these models are trainable even when the full state is not observed [3, 49]. Furthermore, though in full generality preparing quantum Gibbs states is difficult, state preparation has been shown to be efficient in certain regimes relevant to machine learning [49, 4, 84], potentially giving an end-to-end trainable quantum machine learning model. We leave further analytical investigation on the training landscapes of quantum Boltzmann machines to future work.